

Identification of preoptic sleep neurons using retrograde labelling and gene profiling

Shinjae Chung¹, Franz Weber¹, Peng Zhong¹, Chan Lek Tan², Thuc Nghi Nguyen³, Kevin T. Beier⁴, Nikolai Hörmann¹, Wei-Cheng Chang¹, Zhe Zhang¹, Johnny Phong Do¹, Shenqin Yao³, Michael J. Krashes^{5,6}, Bosiljka Tasic³, Ali Cetin³, Hongkui Zeng³, Zachary A. Knight², Liqun Luo⁴ & Yang Dan¹

In humans and other mammalian species, lesions in the preoptic area of the hypothalamus cause profound sleep impairment^{1–5}, indicating a crucial role of the preoptic area in sleep generation. However, the underlying circuit mechanism remains poorly understood. Electrophysiological recordings and c-Fos immunohistochemistry have shown the existence of sleep-active neurons in the preoptic area, especially in the ventrolateral preoptic area and median preoptic nucleus^{6–9}. Pharmacogenetic activation of c-Fos-labelled sleep-active neurons has been shown to induce sleep¹⁰. However, the sleep-active neurons are spatially intermingled with wake-active neurons^{6,7}, making it difficult to target the sleep neurons specifically for circuit analysis. Here we identify a population of preoptic area sleep neurons on the basis of their projection target and discover their molecular markers. Using a lentivirus expressing channelrhodopsin-2 or a light-activated chloride channel for retrograde labelling, bidirectional optogenetic manipulation, and optrode recording, we show that the preoptic area GABAergic neurons projecting to the tuberomammillary nucleus are both sleep active and sleep promoting. Furthermore, translating ribosome affinity purification and single-cell RNA sequencing identify candidate markers for these neurons, and optogenetic and pharmacogenetic manipulations demonstrate that several peptide markers (cholecystokinin, corticotropin-releasing hormone, and tachykinin 1) label sleep-promoting neurons. Together, these findings provide easy genetic access to sleep-promoting preoptic area neurons and a valuable entry point for dissecting the sleep control circuit.

Sleep-active preoptic area (POA) GABAergic (γ -aminobutyric-acid-releasing) neurons labelled by c-Fos immunohistochemistry project to the wake-promoting, histaminergic tuberomammillary nucleus (TMN) in the posterior hypothalamus^{8,9,11,12} (Extended Data Figs 1 and 2). This inhibitory projection is important for sleep generation, since insomnia induced by POA lesion is reversed by muscimol injection into the posterior hypothalamus⁴. To test whether this projection can be used to single out the sleep-promoting neurons, we used a lentivirus pseudotyped with the rabies glycoprotein for retrograde labelling¹³. Injection of the lentivirus with Cre-dependent expression of channelrhodopsin-2 fused with enhanced yellow fluorescent protein (rEIAV-DIO-TLoop-ChR2-eYFP) into the TMN of GAD2-Cre mice led to eYFP labelling of GABAergic neurons in the POA (including the ventrolateral POA, lateral POA, and the lateral part of medial POA), most of which expressed c-Fos following sleep rebound ($73.6 \pm 4.8\%$; Extended Data Fig. 2h, i). These labelled neurons are referred to as GABA^{POA→TMN} neurons.

To test the causal role of GABA^{POA→TMN} neurons in sleep regulation, we optogenetically activated them in freely moving mice. Laser stimulation (2, 5 or 10 Hz, 2 min per trial) was applied every 15–25 min, and wakefulness, rapid eye movement (REM) and non-REM (NREM)

states were classified on the basis of electroencephalogram (EEG) and electromyogram (EMG) recordings (Fig. 1a). GABA^{POA→TMN} neuron activation caused an immediate increase in NREM sleep and a delayed increase in REM sleep at the expense of wakefulness (Fig. 1b, c,

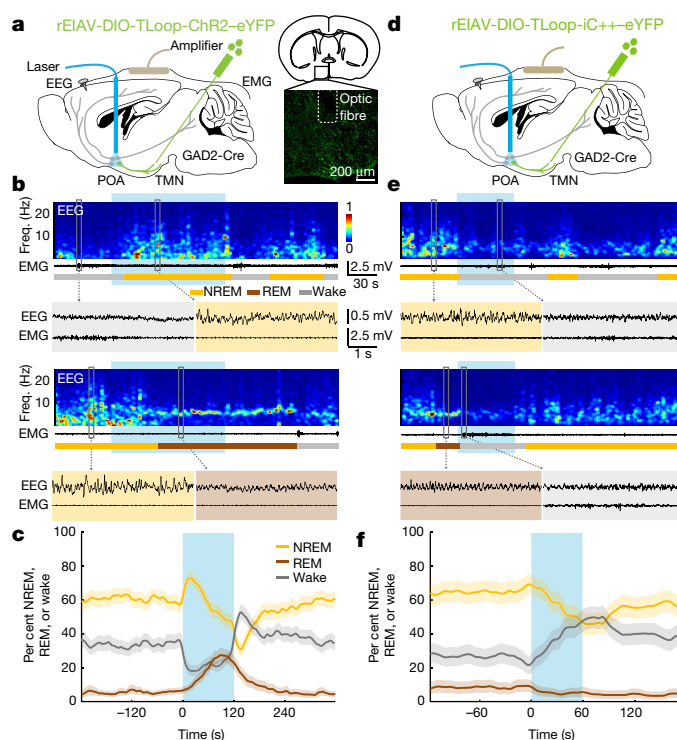


Figure 1 | Optogenetic activation or inhibition of GABA^{POA→TMN} neurons enhances or suppresses sleep. **a**, Schematic of optogenetic activation experiment. Right: fluorescence image of POA (box in schematic) in a GAD2-Cre mouse with rEIAV-DIO-TLoop-ChR2-eYFP injected into the TMN. Mouse brain figure adapted with permission from ref. 31. **b**, Two example trials. Shown are EEG power spectra, EMG traces, brain states (colour coded), and EEG, EMG traces during selected periods (indicated by boxes) on an expanded timescale. Blue shading, laser stimulation (10 Hz, 120 s). Freq., frequency. **c**, Percentage of time in NREM, REM, or wake state before, during, and after laser stimulation (blue shading), averaged from nine mice ($P < 0.0001$ for laser-induced change from wake to sleep states, bootstrap). **d**, Schematic of optogenetic inhibition experiment. **e**, Two example trials. Blue shading, laser stimulation (constant light, 60 s). **f**, Percentage of time in NREM, REM, or wake state before, during, and after laser stimulation, averaged from four mice ($P < 0.0001$ for wake, $P = 0.003$ and 0.002 for REM and NREM, bootstrap). Shading for each trace, 95% confidence interval.

¹Division of Neurobiology, Department of Molecular and Cell Biology, Helen Wills Neuroscience Institute, Howard Hughes Medical Institute, University of California, Berkeley, California 94720, USA. ²Department of Physiology, University of California, San Francisco, San Francisco, California 94158, USA. ³Allen Institute for Brain Science, Seattle, Washington 98103, USA. ⁴Department of Biology, Howard Hughes Medical Institute, Stanford University, Stanford, California 94305, USA. ⁵Diabetes, Endocrinology and Obesity Branch, National Institute of Diabetes and Digestive and Kidney Diseases, National Institutes of Health, Bethesda, Maryland 20892, USA. ⁶National Institute on Drug Abuse, National Institutes of Health, Baltimore, Maryland 21224, USA.

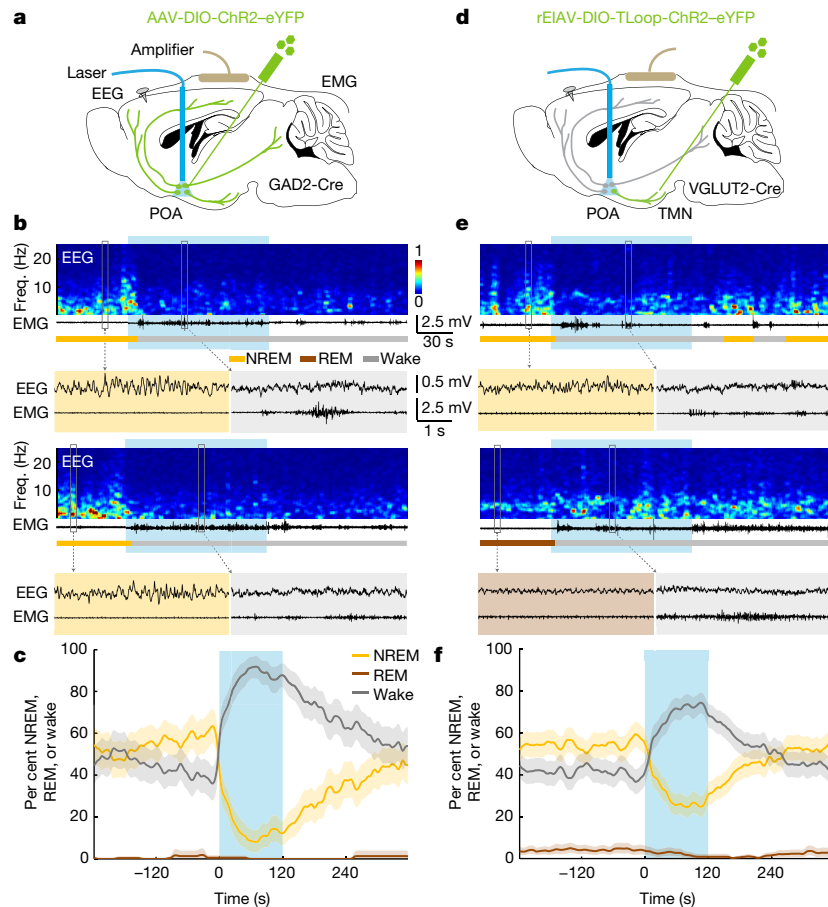


Figure 2 | Optogenetic activation of $GABA^{POA}$ or $VGLUT^{POA \rightarrow TMN}$ neurons promotes wakefulness. **a**, Schematic for optogenetic stimulation of $GABA^{POA}$ neurons. Mouse brain figure adapted with permission from ref. 31. **b**, Two example trials. Blue shading, laser stimulation (10 Hz, 120 s). **c**, Percentage of time in NREM, REM, or wake state, averaged from

five mice ($P < 0.0001$ for increased wakefulness, bootstrap). Shading, 95% confidence interval. **d–f**, Similar to **a–c**, for optogenetic stimulation of $VGLUT^{POA \rightarrow TMN}$ neurons ($P < 0.0001$ for increase in wakefulness, bootstrap, $n = 4$ mice).

Extended Data Fig. 3a–c and Supplementary Video 1). Activating the axons of POA GABAergic ($GABA^{POA}$) neurons (infected by adeno-associated viral vector AAV-DIO-ChR2-eYFP) projecting into the TMN also increased REM and NREM sleep and decreased wakefulness (Extended Data Fig. 4a–g), which could be partly mediated by reduced histamine release (Extended Data Fig. 4h–k). In contrast, inactivating these axons through light-activated chloride channel ($iC++$)¹⁴ caused the opposite effects (Extended Data Fig. 4c).

On the basis of the brain state probability alone (Fig. 1c), however, it is difficult to determine whether the neuronal activity initiates or maintains a particular state, and whether the increased REM sleep results directly from laser stimulation or secondarily from increased NREM sleep, given that animals normally enter REM from NREM sleep. We thus analysed the probability of transitions between each pair of brain states (Extended Data Fig. 5). Laser stimulation of $GABA^{POA \rightarrow TMN}$ neurons significantly enhanced wake \rightarrow NREM and NREM \rightarrow REM transitions but decreased wake \rightarrow wake, NREM \rightarrow wake, and NREM \rightarrow NREM transitions, indicating that activating these neurons enhanced the initiation of both NREM and REM sleep. It also increased REM \rightarrow REM and reduced REM \rightarrow wake transitions, indicating enhanced REM sleep maintenance.

In contrast to ChR2-mediated activation, $iC++$ -mediated silencing of $GABA^{POA \rightarrow TMN}$ neurons strongly increased wakefulness and decreased NREM and REM sleep (Fig. 1d–f). In control mice expressing eYFP alone, laser stimulation had no effect (Extended Data Figs 3d–f and 5c), and the laser-induced changes in sleep and wakefulness were significantly different between the ChR2 and control mice ($P < 0.0001$, bootstrap) and between $iC++$ and control mice ($P = 0.0015$).

To test whether $GABA^{POA \rightarrow TMN}$ neurons are functionally distinct from other nearby neurons, we injected AAV-DIO-ChR2-eYFP into the POA of GAD2-Cre mice (Fig. 2a), which should infect GABAergic neurons irrespective of their projection targets. Optogenetic activation caused an immediate, long-lasting increase in wakefulness (Fig. 2b, c and Supplementary Video 2), through enhanced NREM \rightarrow wake and decreased wake \rightarrow NREM transitions (Extended Data Fig. 5d). Thus, although the POA GABAergic population contains both sleep- and wake-promoting neurons^{6,7}, the effect of non-selective activation is dominated by that of the wake-promoting neurons. We also injected the ChR2-expressing lentivirus into the TMN of VGLUT2-Cre mice (Fig. 2d). Activation of $VGLUT^{POA \rightarrow TMN}$ neurons strongly increased wakefulness (Fig. 2e, f), indicating that the sleep-promoting effect is specific to neurons that are both GABAergic and TMN projecting.

Although c-Fos staining suggests that many $GABA^{POA \rightarrow TMN}$ neurons are sleep active (Extended Data Fig. 2i), c-Fos expression is also modulated by non-activity-related factors. To measure directly the spiking activity of ChR2-labelled $GABA^{POA \rightarrow TMN}$ neurons, we performed optrode recordings in freely moving GAD2-Cre mice. High-frequency laser pulse trains (10 or 20 Hz, 5–10 ms per pulse, 1 s per train) were applied intermittently, and single units exhibiting reliable laser-evoked spiking with short latencies and low jitter were identified as $GABA^{POA \rightarrow TMN}$ neurons (Fig. 3a–c and Extended Data Fig. 6a, b). For the 17 identified neurons, the mean firing rate was significantly higher during REM ($P = 8.5 \times 10^{-4}$, Wilcoxon signed rank test) and NREM ($P = 0.0014$) sleep than wakefulness. Individually, all 17 neurons showed higher firing rates during REM sleep than wakefulness, and 13 of them also showed higher rates during NREM sleep ($P < 0.05$,

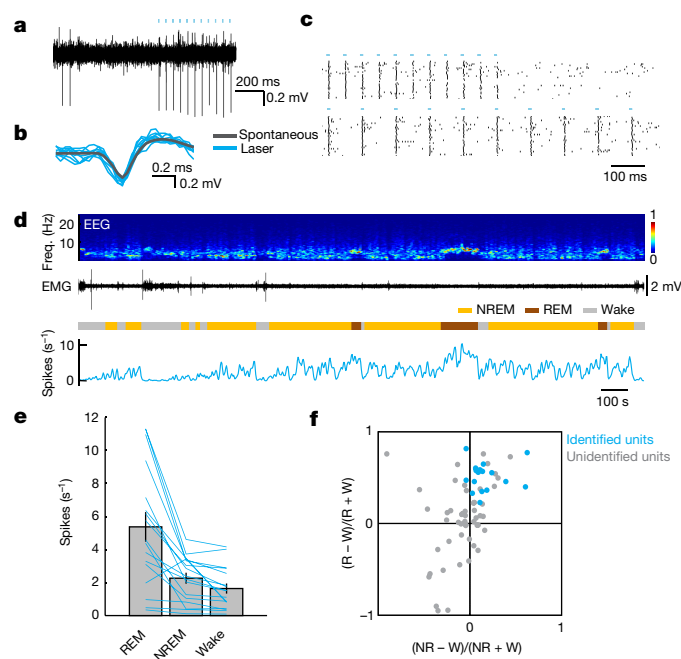


Figure 3 | Optogenetically identified GABA^{POA→TMN} neurons are active during sleep. **a**, Example recording of spontaneous and laser-evoked spikes from a GABA^{POA→TMN} neuron. Blue ticks, laser pulses. **b**, Comparison between laser-evoked (blue) and averaged spontaneous (grey) spike waveforms. **c**, Spike raster showing multiple laser stimulation trials at 10 and 20 Hz. **d**, Firing rates of an example GABA^{POA→TMN} neuron. **e**, Firing rates of 17 identified GABA^{POA→TMN} neurons during different brain states. Each line shows firing rates of one unit; grey bar, average across units. Error bar, \pm s.e.m. **f**, Firing rate modulation of 17 identified (blue, from 7 mice) and 51 unidentified (grey, 11 mice) units. W, wake; R, REM; NR, NREM.

Wilcoxon rank sum test; the remaining four cells showed no significant difference between NREM and wake states; Fig. 3d–f). Within each NREM episode, the activity increased gradually, especially during the episodes preceding REM sleep, and the firing rates were positively correlated with EEG power in the theta (4–12 Hz) and sigma (9–25 Hz) bands but negatively in the gamma (40–120 Hz) band (Extended Data Fig. 6d, e). Compared with these identified GABA^{POA→TMN} neurons, the 51 unidentified POA neurons showed much greater functional diversity (Fig. 3f and Extended Data Fig. 6c), including many that were maximally active during wakefulness^{6,7}.

To explore the circuit mechanisms regulating GABA^{POA→TMN} neuron activity, we mapped their monosynaptic inputs using cell-type-specific tracing the relationship between input and output (cTRIO)¹⁵. We found green fluorescent protein (GFP)-labelled presynaptic neurons in multiple brain regions (Extended Data Fig. 7a, c). Compared with PFC-projecting GABAergic (GABA^{POA→PFC}) neurons, which are wake promoting (Extended Data Fig. 7b), GABA^{POA→TMN} neurons received fewer inputs from the striatum, midbrain, and pons, but more inputs from the hypothalamus and amygdala (Extended Data Fig. 7c). To reveal their collateral projections to other brain areas, we expressed membrane-bound GFP (mGFP) and synaptophysin-mRuby (SYP-mRuby) in GABA^{POA→TMN} neurons. In addition to the TMN, GABA^{POA→TMN} neurons project to several brain areas and probably form local synapses within the POA (Extended Data Fig. 7d–f), suggesting that multiple pathways may contribute to their sleep-promoting effects.

To gain easier genetic access to GABA^{POA→TMN} neurons without relying on retrograde viruses, we next set out to identify their molecular markers. First, we used translating ribosome affinity purification (TRAP)¹⁶ (Fig. 4a and Extended Data Fig. 8a). RNA sequencing (RNA-seq) revealed multiple genes enriched in immunoprecipitated

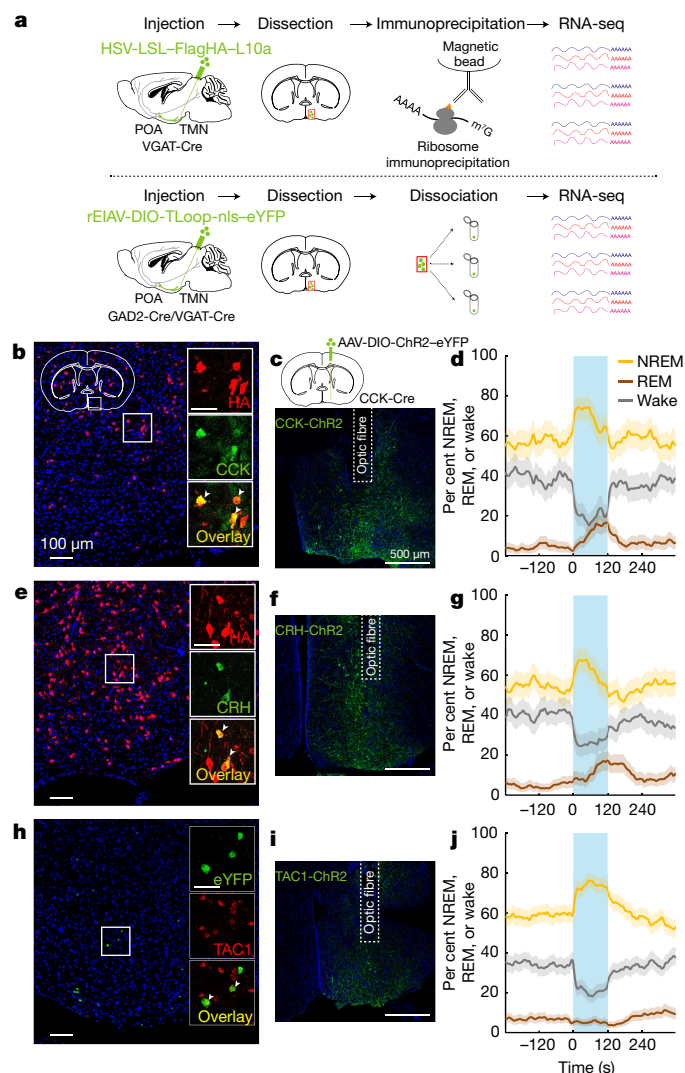


Figure 4 | Identification of molecular markers for POA sleep neurons.

a, Schematics of TRAP (top) and single-cell RNA-seq (bottom) for gene profiling. Mouse brain figure adapted with permission from ref. 31. **b**, Overlap between haemagglutinin (HA) labelling of GABA^{POA→TMN} neurons and CCK expression. Shown is a coronal section at the POA stained with haemagglutinin antibody (red) and Hoechst (blue). Region within the square is magnified (inset; scale bar, 50 μ m). Arrowheads, haemagglutinin-labelled neurons stained with CCK antibody; $49.1 \pm 7.5\%$ of haemagglutinin⁺ neurons are CCK⁺ ($n = 3$ mice). **c**, Schematic of optogenetic activation of POA CCK neurons (top) and a fluorescence image of POA in a CCK-Cre mouse injected with AAV-DIO-ChR2-eYFP. **d**, Percentage of time in NREM, REM, or wake state before, during, and after optogenetic stimulation (blue shading, 10 Hz, 120 s) of CCK neurons ($P = 0.0007$ for REM, $P < 0.0001$ for NREM and wake, bootstrap; $n = 4$ mice). **e**, Overlap between haemagglutinin labelling and CRH expression. $17.1 \pm 1.9\%$ of haemagglutinin-labelled neurons are CRH⁺ (arrowheads; $n = 3$ mice). **f**, Fluorescence image of POA in a CRH-Cre mouse injected with AAV-DIO-ChR2-eYFP. **g**, Percentage of time in NREM, REM, or wake state, averaged from five CRH-Cre mice ($P = 0.0014$ for NREM, $P < 0.0001$ for REM and wake). **h**, Overlap between eYFP labelling of GABA^{POA→TMN} neurons and TAC1 expression. Arrowheads, eYFP⁺ neurons expressing TAC1 (FISH, $n = 2$ mice). **i**, Fluorescence image of POA in a TAC1-Cre mouse injected with AAV-DIO-ChR2-eYFP. **j**, Percentage of time in NREM, REM, or wake state, averaged from seven TAC1-Cre mice ($P < 0.0001$ for NREM and wake). Shading, 95% confidence interval.

RNA from GABA^{POA→TMN} neurons relative to the input RNA (whole lysates before immunoprecipitation; Extended Data Fig. 8b, c and Supplementary Table 1). We focused on the genes encoding neuropeptides, because they play important roles in behavioural regulation

and have proved to be useful markers for specific cell types. Among the highly enriched neuropeptides (Supplementary Table 2), we closely examined corticotropin-releasing hormone (CRH) and cholecystokinin (CCK), both of which have been implicated in sleep regulation^{17,18}. Immunohistochemistry showed that CCK and CRH are expressed in partly overlapping subsets of GABA^{POA→TMN} neurons (Fig. 4b, e and Extended Data Fig. 8e–m).

We then tested whether CCK- or CRH-expressing POA neurons promote sleep. In CCK- and CRH-Cre mice¹⁹ injected with AAV-DIO-ChR2-eYFP into the POA (Fig. 4c, f), laser stimulation significantly decreased wakefulness and increased NREM and REM sleep (Fig. 4d, g and Supplementary Video 3) by enhancing both the initiation and the maintenance of the sleep states (Extended Data Fig. 9a, b). Furthermore, we pharmacogenetically inhibited these neurons by injecting AAV-FLEX-hM4D(Gi)-mCherry into the POA of CCK- or CRH-Cre mice²⁰ (Extended Data Fig. 10a, b). Compared with vehicle injection, clozapine-*N*-oxide (CNO) injection reduced REM and NREM sleep and increased wakefulness in mice expressing hM4D(Gi) but not in control mice (Extended Data Fig. 10a, b). iC⁺⁺-mediated silencing of CCK neurons also reduced REM and NREM sleep and increased wakefulness (Extended Data Fig. 10d).

Notably, we also found significant enrichment of galanin (GAL; Supplementary Table 2), a neuropeptide highly expressed in ventrolateral POA sleep-active neurons^{11,21}. However, optogenetic activation of GAL neurons increased wakefulness and decreased sleep (Extended Data Fig. 10e). This may be because in mice and several other species, GAL is also expressed in some wake-active neurons²¹, and the effect of activating both groups of GAL neurons was dominated by increased wakefulness.

As a complement to TRAP, we also performed single-cell RNA-seq of GABA^{POA→TMN} neurons labelled by rELAV-DIO-TLoop-nls-eYFP (Fig. 4a). We found high-level expression of *Tac1* (Extended Data Fig. 8d). This gene encodes several tachykinin peptides including substance P, which is implicated in sleep regulation²². Fluorescence *in situ* hybridization (FISH) showed *Tac1* expression in $48.4 \pm 8.4\%$ of eYFP-labelled neurons (Fig. 4h), but only in $\sim 10\%$ of GAD1⁺ POA neurons (Extended Data Fig. 8g), confirming its preferential labelling of GABA^{POA→TMN} neurons. In TAC1-Cre mice injected with AAV-DIO-ChR2-eYFP in the POA (Fig. 4i), optogenetic stimulation decreased wakefulness and enhanced NREM sleep (Fig. 4j) by increasing the initiation and maintenance of NREM sleep (Extended Data Fig. 9c). Conversely, pharmacogenetic inhibition of these neurons increased wakefulness and decreased sleep (Extended Data Fig. 10c). Another highly expressed gene is *Pdyn* (Extended Data Fig. 8d), which encodes several opioid peptides including dynorphin A, the infusion of which into the ventrolateral POA increases NREM sleep²³. Optogenetic activation of PDYN neurons also increased NREM sleep and decreased wakefulness (Extended Data Figs 9d, 10f). Notably, although TAC1 partly overlaps with CCK and CRH in the POA (Extended Data Fig. 8j, k, m), the effect of activating TAC1 neurons (increasing only NREM sleep) was different from activating CCK or CRH neurons (increasing both REM and NREM sleep; Fig. 4d, g). This raises the possibility that the GABA^{POA→TMN} population consists of separate subpopulations promoting REM and NREM sleep. In addition, *Tac1* and *Pdyn* were not identified by TRAP, and *Cck* and *Crh* were not identified by single-cell RNA-seq. This suggests that, given the technical limitations of both methods²⁴, using them in parallel can enhance the likelihood of identifying markers for sleep-promoting neurons.

Using optogenetic manipulation and recording, virus-mediated circuit tracing, and gene profiling, we have characterized a population of POA sleep neurons and identified their markers. Similar to previous studies^{6,7}, we observed high functional diversity among unidentified POA neurons. In contrast, all identified GABA^{POA→TMN} neurons were sleep active, forming a much more homogeneous subpopulation (Fig. 3). Whereas activating VGLUT^{POA→TMN} or GABA^{POA} neurons induced wakefulness (Fig. 2), GABA^{POA→TMN} neuron activation strongly

enhanced sleep (Fig. 1). These results emphasize the importance of labelling with both cell-type and projection-target specificity to single out the sleep neurons from their neighbouring wake neurons.

Among the peptide markers enriched in GABA^{POA→TMN} neurons, CCK, CRH, TAC1, and PDYN labelled POA sleep-promoting neurons (Fig. 4 and Extended Data Figs 9 and 10). All four peptides were shown to promote sleep when applied systemically¹⁷, overexpressed in specific brain regions¹⁸, or injected into the POA^{22,23}. However, most POA neurons expressing these markers are likely to co-release GABA (Extended Data Fig. 8e–h). The extent to which their sleep-promoting effects are mediated by GABA versus the neuropeptides remains to be investigated. Moreover, although activation of POA→TMN GABAergic projection can enhance sleep⁴ (Extended Data Fig. 4), the effect of activating the POA sleep neurons may not be mediated by this pathway alone. These neurons project to multiple other areas and form local connections within the POA (Extended Data Fig. 7d–i); whether and how they interact with other sleep–wake control circuits^{25–30} remain to be elucidated. Nevertheless, identification of their molecular markers allows selective targeting of these neurons using readily available Cre mouse lines. Given the plethora of Cre-dependent viral tools and reporter mice for optogenetic/pharmacogenetic manipulations, imaging, and circuit tracing, our findings will greatly facilitate future studies of the sleep control network.

Online Content Methods, along with any additional Extended Data display items and Source Data, are available in the online version of the paper; references unique to these sections appear only in the online paper.

Received 30 November 2016; accepted 6 April 2017.

Published online 17 May 2017.

1. Von Economo, C. Sleep as a problem of localization. *J. Nerv. Ment. Dis.* **71**, 249–259 (1930).
2. Nauta, W. J. Hypothalamic regulation of sleep in rats; an experimental study. *J. Neurophysiol.* **9**, 285–316 (1946).
3. McGinty, D. J. & Sterman, M. B. Sleep suppression after basal forebrain lesions in the cat. *Science* **160**, 1253–1255 (1968).
4. Sallanon, M. et al. Long-lasting insomnia induced by preoptic neuron lesions and its transient reversal by muscimol injection into the posterior hypothalamus in the cat. *Neuroscience* **32**, 669–683 (1989).
5. Lu, J., Greco, M. A., Shiromani, P. & Saper, C. B. Effect of lesions of the ventrolateral preoptic nucleus on NREM and REM sleep. *J. Neurosci.* **20**, 3830–3842 (2000).
6. Szymusiak, R., Alam, N., Steininger, T. L. & McGinty, D. Sleep-waking discharge patterns of ventrolateral preoptic/anterior hypothalamic neurons in rats. *Brain Res.* **803**, 178–188 (1998).
7. Takahashi, K., Lin, J. S. & Sakai, K. Characterization and mapping of sleep-waking specific neurons in the basal forebrain and preoptic hypothalamus in mice. *Neuroscience* **161**, 269–292 (2009).
8. Gong, H. et al. Activation of c-fos in GABAergic neurones in the preoptic area during sleep and in response to sleep deprivation. *J. Physiol. (Lond.)* **556**, 935–946 (2004).
9. Sherin, J. E., Shiromani, P. J., McCarley, R. W. & Saper, C. B. Activation of ventrolateral preoptic neurons during sleep. *Science* **271**, 216–219 (1996).
10. Zhang, Z. et al. Neuronal ensembles sufficient for recovery sleep and the sedative actions of α_2 adrenergic agonists. *Nat. Neurosci.* **18**, 553–561 (2015).
11. Sherin, J. E., Elmquist, J. K., Torrealba, F. & Saper, C. B. Innervation of histaminergic tuberomammillary neurons by GABAergic and galaninergic neurons in the ventrolateral preoptic nucleus of the rat. *J. Neurosci.* **18**, 4705–4721 (1998).
12. Steininger, T. L., Gong, H., McGinty, D. & Szymusiak, R. Subregional organization of preoptic area/anterior hypothalamic projections to arousal-related monoaminergic cell groups. *J. Comp. Neurol.* **429**, 638–653 (2001).
13. Cetin, A. & Callaway, E. M. Optical control of retrogradely infected neurons using drug-regulated “TLoop” lentiviral vectors. *J. Neurophysiol.* **111**, 2150–2159 (2014).
14. Berndt, A. et al. Structural foundations of optogenetics: determinants of channelrhodopsin ion selectivity. *Proc. Natl Acad. Sci. USA* **113**, 822–829 (2016).
15. Beier, K. T. et al. Circuit architecture of VTA dopamine neurons revealed by systematic input-output mapping. *Cell* **162**, 622–634 (2015).
16. Heiman, M. et al. A translational profiling approach for the molecular characterization of CNS cell types. *Cell* **135**, 738–748 (2008).
17. Mansbach, R. S. & Lorenz, D. N. Cholecystokinin (CCK-8) elicits prandial sleep in rats. *Physiol. Behav.* **30**, 179–183 (1983).

18. Kimura, M. *et al.* Conditional corticotropin-releasing hormone overexpression in the mouse forebrain enhances rapid eye movement sleep. *Mol. Psychiatry* **15**, 154–165 (2010).
19. Taniguchi, H. *et al.* A resource of Cre driver lines for genetic targeting of GABAergic neurons in cerebral cortex. *Neuron* **71**, 995–1013 (2011).
20. Sternson, S. M. & Roth, B. L. Chemogenetic tools to interrogate brain functions. *Annu. Rev. Neurosci.* **37**, 387–407 (2014).
21. Gaus, S. E., Strecker, R. E., Tate, B. A., Parker, R. A. & Saper, C. B. Ventrolateral preoptic nucleus contains sleep-active, galaninergic neurons in multiple mammalian species. *Neuroscience* **115**, 285–294 (2002).
22. Zhang, G., Wang, L., Liu, H. & Zhang, J. Substance P promotes sleep in the ventrolateral preoptic area of rats. *Brain Res.* **1028**, 225–232 (2004).
23. Greco, M. A. *et al.* Opioidergic projections to sleep-active neurons in the ventrolateral preoptic nucleus. *Brain Res.* **1245**, 96–107 (2008).
24. Okaty, B. W., Sugino, K. & Nelson, S. B. A quantitative comparison of cell-type-specific microarray gene expression profiling methods in the mouse brain. *PLoS ONE* **6**, e16493 (2011).
25. Weber, F. *et al.* Control of REM sleep by ventral medulla GABAergic neurons. *Nature* **526**, 435–438 (2015).
26. Xu, M. *et al.* Basal forebrain circuit for sleep-wake control. *Nat. Neurosci.* **18**, 1641–1647 (2015).
27. Jegu, S. *et al.* Optogenetic identification of a rapid eye movement sleep modulatory circuit in the hypothalamus. *Nat. Neurosci.* **16**, 1637–1643 (2013).
28. Van Dort, C. J. *et al.* Optogenetic activation of cholinergic neurons in the PPT or LDT induces REM sleep. *Proc. Natl Acad. Sci. USA* **112**, 584–589 (2015).
29. Hayashi, Y. *et al.* Cells of a common developmental origin regulate REM/non-REM sleep and wakefulness in mice. *Science* **350**, 957–961 (2015).
30. Anacleit, C. *et al.* The GABAergic parafacial zone is a medullary slow wave sleep-promoting center. *Nat. Neurosci.* **17**, 1217–1224 (2014).
31. Franklin, K. B. J. & Paxinos, G. in *The Mouse Brain in Stereotaxic Coordinates* 3rd edn, 31–52 (Academic, 2007).

Supplementary Information is available in the online version of the paper.

Acknowledgements We thank J. Cox, L. Pinto for help with sleep recordings; A. Popescu for help with optrode recordings; C. Ma for help with FISH; D. Leib, C. Zimmerman, and D. Estandian for discussions on TRAP; K. Kao, G. Daly, M. Bikov, F. Virani, and G. Carrillo for technical assistance; and C. Koch for supporting the collaboration with the Allen Institute for Brain Science. This work was supported by a Davis Postdoctoral Fellowship (S.C.), Tourette Syndrome Association Grant (S.C.), EMBO Long-term Fellowship (F.W.), Human Frontier Science Program Fellowship (F.W.), and Howard Hughes Medical Institute (Y.D., L.L.).

Author Contributions S.C. and Y.D. conceived and designed the study, and wrote the paper. S.C. performed most of the experiments. F.W. wrote the programs for data analysis and sleep recording, and S.C. and F.W. analysed the data. P.Z. performed slice recordings. C.L.T. and Z.A.K. constructed the herpes simplex virus (HSV virus), and performed TRAP experiments. T.N., B.T., and H.Z. performed single-cell RNA-seq. K.T.B. and L.L. provided cTRIO and axon arborization analysis reagents and performed part of the input tracing experiments. N.H. and Z.Z. performed FISH. W.C.C. and J.P.D. performed part of the sleep recording. M.J.K. generated PDYN-IRES-Cre mice. S.Y. and A.C. constructed the lentivirus. Y.D. supervised all aspects of the work.

Author Information Reprints and permissions information is available at www.nature.com/reprints. The authors declare no competing financial interests. Readers are welcome to comment on the online version of the paper. Publisher's note: Springer Nature remains neutral with regard to jurisdictional claims in published maps and institutional affiliations. Correspondence and requests for materials should be addressed to Y.D. (ydan@berkeley.edu).

Reviewer Information *Nature* thanks M. Halassa, T. Kilduff, A. Yamanaka and the other anonymous reviewer(s) for their contribution to the peer review of this work.

METHODS

Animals. GAD2-IRES-Cre, VGLUT2-IRES-Cre, VGAT-IRES-Cre, GAD1-eGFP, CCK-IRES-Cre, CRH-IRES-Cre, TAC1-IRES-Cre, and HDC-IRES-Cre mice (Jackson stock numbers 010802, 016963, 016962, 007677, 012706, 012704, 021877, and 021198, respectively) were obtained from Jackson Laboratory^{19,32,33} and VGLUT2-eGFP mice were from MMRRC (MMRRC 011835-UCD). PDYN-IRES-Cre mice were obtained from Bradford Lowell³⁴. GAL-Cre mice were obtained from GENSAT (stock number K187). Mice were housed in 12 h light–dark cycle (lights on 7:00 and off at 19:00) with free access to food and water. Experiments were performed in adult male or female mice (6–12 weeks old). All procedures were approved by Institutional Animal Care and Use Committees of the University of California, Berkeley, University of California, San Francisco, Allen Institute for Brain Science, and Stanford University and were done in accordance with federal regulations and guidelines on animal experimentation.

Note that, in different experiments, GAD1, GAD2, and VGAT were used to identify GABAergic neurons. To examine the relationship between GAD1, GAD2, and VGAT in the POA, we quantified the overlap between GAD1 and VGAT on the basis of the double *in situ* hybridization data from the Allen Mouse Brain Atlas (<http://connectivity.brain-map.org/transgenic/experiment/100142488>) and found that 95% (327 out of 345) of VGAT-positive neurons also contained GAD1. Comparison between GAD1 and GAD2 expression in the POA (<http://connectivity.brain-map.org/transgenic/experiment/100142491>) showed that 99% (246 out of 248) of GAD1 neurons also contained GAD2. Together, these data indicate a very high degree of overlap between GAD1, GAD2, and VGAT in the POA.

Virus preparation. AAV₂-EF1 α -DIO-ChR2-eYFP and AAV₈-hSyn-FLEX-hM4D(Gi)-mCherry were obtained from the University of North Carolina vector core. The final titre was estimated to be $\sim 10^{12}$ genome copies per millilitre. AAV_{DJ}-EF1 α -DIO-ChR2-eYFP, AAV_{DJ}-EF1 α -DIO-eYFP, AAV₈-EF1 α -DIO-iC $^{++}$ -eYFP, and AAV_{DJ}-EF1 α -DIO-iC $^{++}$ -eYFP were obtained from Stanford University virus core. Lentivirus rEIAV-DIO-TLoop-ChR2-eYFP, rEIAV-DIO-TLoop-iC $^{++}$ -eYFP, and rEIAV-DIO-TLoop-nls-eYFP were obtained from Salk virus core and Allen Institute for Brain Science¹³. Rabies-tracing reagents (AAV-CAG-FLEX^{loxP}-TVA-mCherry, AAV-CAG-FLEX^{loxP}-RG, rabies glycoprotein) and EnvA-pseudotyped, rabies-glycoprotein-deleted, and GFP-expressing rabies viral particles (RVdG), cTRIO reagents (CAV-FLEX^{loxP}-Flp, AAV-FLEX^{FRT}-TVA-mCherry, AAV-FLEX^{FRT}-RG, and EnvA-pseudotyped, rabies-glycoprotein-deleted, and GFP-expressing rabies viral particles (RVdG)) and axon arborization analysis reagents (CAV-FLEX^{loxP}-Flp and AAV-hSyn1-FLEX^{FRT}-mGFP-2A-synaptophysin-mRuby) were obtained from Stanford University¹⁵. HSV-LoxSTOPLox-FlagHA-L10a was obtained from the University of California, San Francisco.

Sequence for nls-eYFP used in rEIAV-DIO-TLoop-nls-eYFP. The sequence was ATGCTAGATAAGCCCCCAAGAAGAAGAGGAAGGTGGCCGC CACCATGGTGAAGCAAGGGCGAGGAGCTGTTCACCGGGTGGTGCCCA TCCTGGTCGAGCTGGACGGCGACGTAACGGCCACAAGTTCAGCGTG TCCGGCGAGGGCGAGGGCGATGCCACCTACGGCAAGCTGACCCTGAA GTTCATCTGCACCAACGGCAAGCTGCCCGTGGCCCTGGCCACCCCTCGT GACCACCTTCGGCTACGGCGCTGAGTCTTCGCCCCGTACCCCGAC CACATGAAGCAGCAGCACTTCTCAAGTCCGCGATGCCGCAAGGCTACG TCCAGGAGCGCACCATCTTCTCAAGGACGACGGCAACTACAAGACC CGCGCCGAGGTGAAGTTCGAGGGCGACACCCTGGTGAACCGCATCGAG CTGAAGGGCATCGACTTCAAGGAGGACGGCAACATCTGGGGCACAA GCTGGAGTACAACACTACAACAGCCACAACGCTCTATATCATGGCCGACAA GCAGAAGAAGCGGCAAGGTGAAGTCAAGATCCGCCACAACATCG AGGACGGCAGCGTGCAGCTCGCCGACCACTACCAGCAGAACACCCCCA TCGGCGACGGCCCCGTGCTGCTGCCGACAACCACTACCTGAGCTAC CAGTCCGCCCTGAGCAAAGACCCCAACGAGAAGCGGATCACATGGT CCTGTGGAGTTCGTGACCGCCGCGGGATCACTCTCGGCATGGACG AGCTGTAAGAAGTAAAA.

Surgery. Mice of a specific genotype were randomly assigned to experimental and control groups. Experimental and control animals were subjected to exactly the same surgical and behavioural manipulations. Data from animals used in experiments were excluded on the basis of histological criteria that included injection sites, virus expression, and optical fibre placement. Only animals with injection sites and optic fibre placement in the region of interest were included.

To implant EEG and EMG recording electrodes, adult mice (6–12 weeks old) were anaesthetized with 1.5–2% isoflurane and placed on a stereotaxic frame. Two stainless steel screws were inserted into the skull 1.5 mm from midline and 1.5 mm anterior to the bregma, and two others were inserted 3 mm from midline and 3.5 mm posterior to the bregma. Two EMG electrodes were inserted into the neck musculature. Insulated leads from the EEG and EMG electrodes were soldered to a 2 \times 3-pin header, which was secured to the skull using dental cement.

For optogenetic activation/inhibition experiments, a craniotomy was made on top of the target region for optogenetic manipulation in the same surgery as for EEG and EMG implant, and 0.1–0.5 μ l virus was injected into the target region using Nanoject II (Drummond Scientific) via a micropipette. We then implanted optic fibres bilaterally into the target region. Dental cement was applied to cover the exposed skull completely and to secure the implants for EEG and EMG recordings to the screws. After surgery, mice were allowed to recover for at least 2–3 weeks before experiments. For anti-histamine experiments (Extended Data Fig. 4), triprolidine (Tocris) was administered intraperitoneally at 20 mg per kg (body weight) and brain states were recorded for 3 h.

For retrograde tracing in Extended Data Fig. 1a, 0.2–0.3 μ l red or green RetroBeads (Lumafluor) was injected into each target region.

For optrode recording experiments, the optrode assembly was inserted into the POA at a depth of 4.9 mm. Screws were attached to the skull for EEG recordings, and an EMG electrode was inserted into the neck musculature. The optrode assembly, screws, and EEG/EMG electrodes were secured to the skull using dental cement. These procedures are related to the results in Fig. 3 and Extended Data Fig. 6.

For rabies tracing, AAV-CAG-FLEX^{loxP}-TVA-mCherry and AAV-CAG-FLEX^{loxP}-RG were injected into the TMN of HDC-Cre mice. Two to three weeks later, EnvA-pseudotyped, glycoprotein-deleted, and GFP-expressing rabies viral particles (RVdG) were injected into the TMN, and mice were euthanized 1 week later. These procedures are related to the results in Extended Data Fig. 2.

For cTRIO experiments, a retrograde virus CAV-FLEX^{loxP}-Flp (5.0×10^{12} genome copies per millilitre) was injected into either the TMN or the PFC of GAD2-Cre mice to express Flp recombinase specifically in GABA^{POA \rightarrow PFC} or GABA^{POA \rightarrow PFC} neurons, and AAV-FLEX^{FRT}-TVA-mCherry (2.6×10^{12} genome copies per millilitre) and AAV-FLEX^{FRT}-RG (1.3×10^{12} genome copies per millilitre) were injected into the POA to express TVA (the receptor for the EnvA envelope glycoprotein)-mCherry and rabies glycoprotein in the Flp-expressing neurons. Two to three weeks later, EnvA-pseudotyped, glycoprotein-deleted, and GFP-expressing rabies viral particles (RVdG) (5.0×10^8 colony forming units per millilitre) were injected into the POA, and mice were euthanized 1 week later for histology. These procedures are related to the results in Extended Data Fig. 7.

For axon arborization experiments, CAV-FLEX^{loxP}-Flp was injected into TMN, and AAV-hSyn1-FLEX^{FRT}-mGFP-2A-synaptophysin-mRuby was injected into the POA of GAD2-Cre mice. Mice were euthanized 4–7 weeks later for histology. These procedures are related to the results in Extended Data Fig. 7.

For pharmacogenetic experiments, AAV₈-hSyn-FLEX-hM4D(Gi)-mCherry was injected bilaterally into the POA. These procedures are related to the results in Extended Data Fig. 10.

For TRAP experiments, we injected Cre-inducible HSV expressing the large ribosomal subunit protein Rpl10a fused with Flag/haemagglutinin tag (HSV-LoxSTOPLox-FlagHA-L10a) into the TMN of VGAT-Cre mice. After 30–45 days of expression, the POA was dissected, and ribosome immunoprecipitation was performed to pull down the messenger RNAs (mRNAs) attached to Rpl10a. These procedures are related to the results in Fig. 4 and Extended Data Fig. 8.

For single-cell RNA-seq experiments, rEIAV-DIO-TLoop-nls-eYFP was injected into the TMN of GAD2-Cre and VGAT-Cre mice. Four weeks later, we dissociated eYFP-labelled POA neurons for single-cell RNA-seq. These procedures are related to the results in Fig. 4 and Extended Data Fig. 8.

For immunohistochemistry-detecting peptides, mice received a single intraventricular injection of colchicine (12 μ g) 1–2 days before killing. These procedures are related to the results in Fig. 4.

The stereotaxic coordinates were as follows. TMN: anteroposterior (AP) – 2.45 mm, mediolateral (ML) 1 mm, dorsoventral (DV) 5–5.2 mm from the cortical surface; POA: AP 0 mm, ML 0.7 mm, DV 5.2 mm; PFC: AP +2.0 mm, ML 0.4 mm, DV 2 mm; vLPAG: AP –4.7 mm, ML 0.7 mm, DV 2.3 mm; dorsomedial hypothalamus: AP –1.8 mm, ML 0.4 mm, DV 5.2 mm; habenula: AP –1.8 mm, ML 0.5 mm, DV 2.2 mm.

Sleep deprivation and sleep rebound experiment. Sleep deprivation started at the beginning of the light period (7:00) and lasted till 13:00. Mice were kept awake by a combination of cage tapping, introduction of foreign objects such as paper towels, cage rotation, and fur stroking with a paintbrush³⁵, gentle handling procedures that have been used extensively to induce sleep deprivation³⁶. EEG and EMG were not recorded during sleep deprivation and recovery. After 6 h of deprivation, sleep-deprived mice were allowed rebound sleep for 4 h before being euthanized by cervical dislocation and decapitation. c-Fos immunohistochemistry was performed as described below. These procedures are related to the results in Extended Data Figs 1 and 2.

Sleep recording. Behavioural experiments were performed in home cages placed in sound-attenuating boxes. Sleep recordings were performed between 12:00 and

19:00 (light on at 7:00 and off at 19:00). EEG and EMG electrodes were connected to flexible recording cables via a mini-connector. EEG and EMG signals were recorded and amplified using AM Systems, digitally filtered (0.1–1,000 Hz and 10–1,000 Hz for EEG and EMG recordings respectively), and digitized at 600 Hz using LabView. Spectral analysis was performed using fast Fourier transform, and brain states were classified into NREM, REM, and wake states (wake: desynchronized EEG and high EMG activity; NREM: synchronized EEG with high-amplitude, low-frequency (0.5–4 Hz) activity and low EMG activity; REM: high power at theta frequencies (6–9 Hz) and low EMG activity). Brain states were classified into NREM sleep, REM sleep, and wakefulness using custom-written MATLAB software, and the classification was performed without any information about the identity of the animal or laser stimulation timing as previously described²⁵.

Optogenetic manipulation. Each optic fibre (200 µm diameter; Thorlabs) was attached through an FC/PC adaptor to a 473-nm blue laser diode (Shanghai laser), and light pulses were generated using a Master 8 (A.M.P.I.). All photostimulation/inhibition experiments were conducted bilaterally and fibre optic cables were connected at least 2 h before the experiments for habituation. For photostimulation/inhibition experiments in ChR2-, iC⁺+, or eYFP-expressing mice, light pulses (10 ms per pulse, 10 Hz, 4–8 mW) or step pulses (60 s) were triggered using Master 8 that provided simultaneous input into two blue lasers. In each optogenetic manipulation experiment, inter-stimulation interval for optogenetic manipulation was chosen randomly from a uniform distribution between 15 and 25 min.

Optrode recordings. Custom-made optrodes³⁷ consisted of an optic fibre (200 µm in diameter) glued together with six pairs of stereotrodes. Two FeNiCr wires (Stablohm 675, California Fine Wire) were twisted together and electroplated to an impedance of ~600 kΩ using a custom-built plating device. The optrode was attached to a driver to allow vertical movement of the optrode assembly. The optrode was slowly lowered to search for light-responsive neurons. Wires to record cortical EEG and EMG from neck musculatures were also attached for simultaneous recordings. A TDT RZ5 amplifier was used for all the recordings, signals were filtered (0.3–8 kHz) and digitized at 25 kHz. At the end of the experiment, an electrolytic lesion was made by passing a current (100 µA, 10 s) through one or two electrodes to identify the end of the recording tract.

Spikes were sorted offline on the basis of the waveform energy and the first three principal components of the spike waveform on each stereotrode channel. For single unit isolation, all channels were separated into groups and spike waveforms were identified either manually using Klusters (<http://neurosuite.sourceforge.net/>) or automatically using the software klustakwik (<http://klustakwik.sourceforge.net/>). The quality of each unit was assessed by the presence of a refractory period and quantified using isolation distance and L_{ratio} . Units with an isolation distance <20 and L_{ratio} >0.1 were discarded³⁸.

To identify ChR2-tagged neurons, laser pulse trains (10 and/or 20 Hz) were delivered intermittently every minute. A unit was identified as ChR2-expressing if spikes were evoked by laser pulses with short first-spike latency (<6 ms for all units in our sample) and the waveforms of the laser-evoked and spontaneous spikes were highly similar (correlation coefficient >0.9). Mean latency of all identified units was 3.05 ms. Mean correlation coefficient of all identified units was 0.99. To calculate the average firing rate of each unit in each brain state, spikes during the laser pulse trains were excluded. These procedures are related to the results in Fig. 3 and Extended Data Fig. 6.

Immunohistochemistry. Mice were deeply anaesthetized and transcardially perfused using PBS buffer followed by 4% paraformaldehyde in PBS. Brains were post-fixed in fixative and stored in 30% sucrose in PBS overnight for cryoprotection. Brains were embedded and mounted with Tissue-Tek OCT compound (Sakura Finetek) and 20 µm sections were cut using a cryostat (Leica). Brain slices were washed using PBS, permeabilized using PBST (0.3% Triton X-100 in PBS) for 30 min and then incubated with blocking solution (5% normal goat serum or normal donkey serum in PBST) for 1 h followed by primary antibody incubation overnight at 4°C using the following antibodies: anti-GFP antibody (A-11122 or A-11120, Life technologies, 1:1,000); anti-cFos antibody (sc-52-G and sc-52, Santa Cruz Biotech, 1:1,000); anti-CKK-8 antibody (20078, Immunostar, 1:500); anti-CRH antibody (sc-1759, Santa Cruz Biotech, 1:500); anti-haemagglutinin antibody (C29F4, Cell Signaling tech, 1:1,000); and anti-HDC antibody (16045, Progen, 1:1,000).

The next day, slices were washed with PBS and incubated with appropriate secondary antibodies for 2 h (1:500, all from Invitrogen): A-11008, Alexa Fluor 488 goat anti-rabbit IgG; A-21206, Alexa Fluor 488 donkey anti-rabbit IgG; A-11055, Alexa Fluor 488 donkey anti-goat IgG; A-21202, Alexa Fluor 488 donkey anti-mouse IgG; A-11012, Alexa Fluor 594 goat anti-rabbit IgG; A-21207, Alexa Fluor 594 donkey anti-rabbit IgG; A-11058, Alexa Fluor 594 donkey anti-goat IgG; A-21245, Alexa Fluor 647 goat anti-rabbit IgG.

The slices were washed with PBS followed by counterstaining with DAPI or Hoechst and coverslipped. Fluorescence images were taken using a confocal microscope (LSM 710 AxioObserver Inverted 34-Channel Confocal, Zeiss) or Nanozoomer (Hamamatsu).

FISH. FISH was performed with two methods. First, FISH for CCK, CRH, TAC1, and GAD1 was done using RNAscope assays according to the manufacturer's instructions (Advanced Cell Diagnostics). Second, to make TAC1, GAD1, and GAD2 FISH probes, DNA fragments containing the coding or untranslated sequences were amplified using PCR from mouse whole brain complementary DNA (cDNA) (Zyagen). A T7 RNA polymerase recognition site was added to the 3' end of the PCR product. The PCR product was purified using a PCR purification kit (Qiagen). One microgram of DNA was used for *in vitro* transcription by using digoxigenin (DIG) RNA labelling mix (Roche) and T7 RNA polymerase. After DNase I treatment for 30 min at 37°C, the RNA probe was purified using probeQuant G-50 Columns (GE Healthcare). Sections (20 µm) were pre-treated with proteinase K (0.1 µg ml⁻¹), acetylated, dehydrated through ethanol (50, 70, 95, and 100%), and air dried. Pre-treated sections were then incubated for 16–20 h at 60°C, in a hybridization buffer containing sense or anti-sense riboprobes. After the sections were hybridized, they were treated with RNase A (20 µg ml⁻¹) for 30 min at 37°C and then washed four times in decreasing salinity (from 2× to 0.1× standard saline citrate buffer) and a 30 min wash at 68°C. Sections were incubated with 3% hydrogen peroxide in PBS for 1 h and washed using PBS. After incubation in the blocking buffer for 1 h (TNB buffer, Perkin Elmer), sections were incubated with anti-DIG-POD antibody (1:500, Roche) in TNB buffer for 2 h. TSA-plus-Fluorescein reagent was used to visualize the signal. For GAD-FISH, anti-DIG-AP antibody (1:500, Roche) and Fast Red TR/Naphthol AS-MX (F4523, Sigma-Aldrich) were used to visualize the signal. After washing the sections in PBS, they were incubated with blocking buffer for 2 h followed by incubation with anti-GFP antibody overnight, and finally incubated with a secondary antibody as described above. To examine the overlap between each peptide marker and GAD, we used CCK-, CRH-, TAC1-, and PDYN-Cre mice injected with AAV-EF1α-DIO-ChR2-eYFP or AAV-EF1α-DIO-eYFP. These procedures are related to the results in Extended Data Figs 2 and 8.

CTRIO data analysis. For analysis of rabies-tracing data, consecutive 60 µm coronal sections were collected and stained using Hoechst. Slides were scanned using Nanozoomer (Hamamatsu). GFP⁺ input neurons were counted from the forebrain to the posterior brainstem except sections adjacent to the injection sites (1 mm from the injection site), and grouped into ten regions based on Allen Mouse Brain Atlas (<http://mouse.brain-map.org/static/atlas>) using anatomical landmarks in the sections visualized by Hoechst staining and autofluorescence. We normalized the number of neurons in each region by the total number of input neurons in the entire brain. These procedures are related to the results in Extended Data Fig. 7.

Axon arborization analysis. Consecutive 60 µm coronal sections were collected and stained using Hoechst. Slides were scanned using a Nanozoomer (Hamamatsu). All images were acquired using identical settings and were analysed using ImageJ as previously described¹⁵. Images were background subtracted (rolling ball radius of 50 pixels), thresholded, and pixels above this threshold were interpreted as positive signals. The mGFP- or eYFP-labelled axon arborization signal was measured for each region and averaged across the five sections. These procedures are related to the results in Extended Data Fig. 7.

TRAP. We adapted a previously described procedure to perform TRAP experiment³⁹. Mice were euthanized at 12:00 to 14:00 and the POA was rapidly dissected on ice with a dissection buffer (1× HBSS, 2.5 mM HEPES (pH 7.4), 4 mM NaHCO₃, 35 mM glucose, 100 µg ml⁻¹ cycloheximide). Brains from six mice were then pooled, homogenized in the homogenization buffer (10 mM HEPES (pH 7.4), 150 mM KCl, 5 mM MgCl₂, 100 nM calyculin A, 2 mM DTT, 100 U ml⁻¹ RNasin, 100 µg ml⁻¹ cycloheximide and protease). Homogenates were transferred to a microcentrifuge tube and clarified at 2,000g for 10 min at 4°C. The supernatant was transferred to a new tube, and 70 µl of 10% NP40 and 70 µl of 1,2-diheptanoyl-*sn*-glycero-3-phosphocholine (DHPC, 300 mM) per millilitre of supernatant were added. This solution was mixed and then clarified at 17,000g for 10 min at 4°C. The resulting high-speed supernatant was transferred to a new tube. This supernatant served as the input. A small amount (25 µl) was added to a new tube containing 350 µl of buffer RLT for future input RNA purification.

Immunoprecipitation was performed with an anti-Flag antibody loaded beads. The beads were washed four times using 0.15 M KCl Wash buffer (10 mM HEPES (pH 7.4), 350 mM KCl, 5 mM MgCl₂, 2 mM DTT, 1% NP40, 100 U ml⁻¹ RNasin, and 100 µg ml⁻¹ cycloheximide). After the final wash, the RNA was eluted by addition of buffer RLT (350 µl) to the beads on ice, the beads removed by a magnet, and the RNA purified using the RNeasy Micro Kit (Qiagen) and analysed using an Agilent 2100 Bioanalyzer. cDNA libraries for RNA-seq were prepared with Ovation RNA-Seq System V2 and Ovation Ultralow Library Systems (NuGen), and

analysed on an Illumina HiSeq 2500. Gene classification shown in Supplementary Table 1 was performed using PANTHER (<http://pantherdb.org/>)⁴⁰. These procedures are related to the results in Fig. 4 and Extended Data Fig. 8.

Single-cell RNA-seq. We adapted a previously described procedure to isolate fluorescently labelled neurons from the mouse brain^{41–43}.

Single-cell isolation. Individual adult male mice (postnatal day 56 ± 3) were anaesthetized in an isoflurane chamber, decapitated, and the brain was immediately removed and submerged in fresh ice-cold artificial cerebrospinal fluid (ACSF) containing 126 mM NaCl, 20 mM NaHCO₃, 20 mM dextrose, 3 mM KCl, 1.25 mM NaH₂PO₄, 2 mM CaCl₂, 2 mM MgCl₂, 50 μM DL-AP5 sodium salt, 20 μM DNQX, and 0.1 μM tetrodotoxin, bubbled with a carbogen gas (95% O₂ and 5% CO₂). The brain was sectioned on a vibratome (Leica VT1000S) on ice, and each slice (300–400 μm) was immediately transferred to an ACSF bath at room temperature. After the brain slicing was complete (not more than 15 min), individual slices of interest were transferred to a small Petri dish containing bubbled ACSF at room temperature. The POA was microdissected under a fluorescence dissecting microscope, and the slices before and after dissection were imaged to examine the location of the microdissected tissue and confirm its location. The dissected tissue pieces were transferred to a microcentrifuge tube and treated with 1 mg ml^{−1} pronase (Sigma, P6911-1G) in carbogen-bubbled ACSF for 70 min at room temperature without mixing in a closed tube. After incubation, with the tissue pieces sitting at the bottom of the tube, the pronase solution was pipetted out of the tube and exchanged with cold ACSF containing 1% fetal bovine serum. The tissue pieces were dissociated into single cells by gentle trituration through Pasteur pipettes with polished tips of 600, 300, and 150 μm diameter. Single cells were isolated by fluorescence-activated cell sorting into individual wells of 96-well plates or 8-well PCR strips containing 2.275 μl of Dilution Buffer (SMARTer Ultra Low RNA Kit for Illumina Sequencing, Clontech 634936), 0.125 μl RNase inhibitor (SMARTer kit), and 0.1 μl of 1:1,000,000 diluted RNA spike-in RNAs (ERCC RNA Spike-In Mix 1, Life Technologies 4456740). Sorting was performed on a BD FACSARIA SORP using a 130 μm nozzle, a sheath pressure of 10 p.s.i., and in the single-cell sorting mode. To exclude dead cells, DAPI (DAPI*2HCl, Life Technologies D1306) was added to the single-cell suspension to the final concentration of 2 ng ml^{−1}. Sorted cells were frozen immediately on dry ice and stored at −80 °C.

cDNA amplification and library construction. We used the SMARTer kit described above to reverse transcribe single-cell RNA and amplify the cDNA for 19 PCR cycles. To stabilize the RNA after quickly thawing the cells on ice, we immediately added to each sample an additional 0.125 μl of RNase inhibitor mixed with SMART CDS Primer II A. All steps downstream were performed according to the manufacturer's instructions. cDNA concentration was quantified using Agilent Bioanalyzer High Sensitivity DNA chips. For most samples, 1 ng of amplified cDNA was used as input to make sequencing libraries with a Nextera XT DNA kit (Illumina FC-131-1096). Individual libraries were quantified using Agilent Bioanalyzer DNA 7500 chips. To assess sample quality and adjust the concentrations of libraries for multiplexing on HiSeq, all libraries were sequenced first on Illumina MiSeq to obtain approximately 100,000 reads per library, and then on Illumina HiSeq 2000 or 2500 to generate 100 base pair reads. These procedures are related to the results in Fig. 4 and Extended Data Fig. 8.

Strategy for marker identification. Since both TRAP and single-cell RNA-seq have technical limitations and are prone to false-positive and false-negative errors, we used the following strategy for identifying markers for POA sleep neurons. (1) To eliminate false-positive errors, the candidate markers with existing Cre lines were tested in optogenetic experiments, and cell types that did not promote sleep were eliminated (for example, GAL, which was found to be enriched in the TRAP experiment). (2) To reduce false-negative errors, we included markers identified by either method in our candidate list, rather than only those identified by both methods. This should have enhanced our chance of finding a useful marker, even if it were missed by one of the methods because of false-negative errors. Of course, this strategy could increase the probability for false-positive errors in our candidate list, but these errors were eliminated by the functional test in (1).

Pharmacogenetic manipulation. To inhibit CCK, CRH, or TAC1 neurons, we injected CNO dissolved in 0.1 ml vehicle solution (PBS with 0.5% dimethyl sulfoxide (DMSO)) into CCK-, CRH- or TAC1-Cre mice expressing hM4Di in the POA, 20 min before the recording session. CNO was administered intraperitoneally at 2.5 mg per kg (body weight). Vehicle solution was injected for the control experiment. These procedures are related to the results in Extended Data Fig. 10.

Slice recording. Slice recordings were made at postnatal days 42–50. AAV_{DJ}-EF1α-DIO-ChR2-eYFP (500 nl) was injected into the POA of GAD2-Cre mice, and recording was made 2–3 weeks after injection. Slice preparation was according to procedures described previously⁴⁴. A mouse was deeply anaesthetized with 5% isoflurane. After decapitation, the brain was dissected rapidly and placed in ice-cold oxygenated HEPES-buffered ACSF (in mM: NaCl 92, KCl 2.5, NaH₂PO₄

1.2, NaHCO₃ 30, HEPES 20, glucose 25, sodium ascorbate 5, thiourea 2, sodium pyruvate 3, MgSO₄·7H₂O 10, CaCl₂·2H₂O 0.5, and NAC 12, at pH 7.4, adjusted with 10 M NaOH), and coronal sections of the TMN were made with a vibratome (Leica). Slices (300 μm thick) were recovered in oxygenated NMDG-HEPES solution (in mM: NMDG 93, KCl 2.5, NaH₂PO₄ 1.2, NaHCO₃ 30, HEPES 20, glucose 25, sodium ascorbate 5, thiourea 2, sodium pyruvate 3, MgSO₄·7H₂O 10, CaCl₂·2H₂O 0.5, and NAC 12, at pH 7.4, adjusted with HCl) at 32 °C for 10 min and then maintained in an incubation chamber with oxygenated standard ACSF (in mM: NaCl 125, KCl 3, CaCl₂ 2, MgSO₄ 2, NaH₂PO₄ 1.25, sodium ascorbate 1.3, sodium pyruvate 0.6, NaHCO₃ 26, glucose 10, and NAC 10, at pH 7.4, adjusted by 10 M NaOH) at 25 °C for 1–4 h before recording. All chemicals were from Sigma.

Whole-cell recordings were made at 30 °C in oxygenated solution (in mM: NaCl 125, KCl 4, CaCl₂ 2, MgSO₄ 1, NaH₂PO₄ 1.25, sodium ascorbate 1.3, sodium pyruvate 0.6, NaHCO₃ 26, and glucose 10, at pH 7.4). Inhibitory postsynaptic currents were recorded using a caesium-based internal solution (in mM: CsMeSO₄ 125, CsCl 2, HEPES 10, EGTA 0.5, MgATP 4, Na₂GTP 0.3, sodium phosphocreatine 10, TEACl 5, QX-314 3.5, at pH 7.3, adjusted with CsOH, 290–300 mOsm) and isolated by clamping the membrane potential of the recorded neuron at the reversal potential of the excitatory synaptic currents. The resistance of the patch pipette was 3–5 MΩ. The cells were excluded if the series resistance exceeded 40 MΩ or varied by more than 20% during the recording period. To activate ChR2, we used a mercury arc lamp (Olympus) coupled to the epifluorescence light path and bandpass filtered at 450–490 nm (Semrock), gated by an electromagnetic shutter (Uniblitz). A blue light pulse (5 ms) was delivered through a 40 × 0.8 numerical aperture water immersion lens (Olympus) at a power of 1–2 mW. Data were recorded with a Multiclamp 700B amplifier (Axon instruments) filtered at 2 kHz and digitized with a Digidata 1440A (Axon instruments) at 4 kHz. Recordings were analysed using Clampfit (Axon instruments). These procedures are related to the results in Extended Data Fig. 2.

Single-cell reverse-transcription PCR. At the end of each recording, cytoplasm was aspirated into the patch pipette, expelled into a PCR tube as described previously⁴⁵. The single-cell reverse-transcription PCR (RT-PCR) protocol was designed to detect the presence of mRNAs coding for GAPDH, GAD1, VGLUT2, and HDC. First, reverse transcription and the first round of PCR amplification were performed with gene-specific multiplex primer using the SuperScript III One-Step RT-PCR kit (12574-018, Invitrogen) according to the manufacturer's protocol. Second, nested PCR was performed using GoTaq Green Master Mix (M7121, Promega) with nested primers for each gene. Amplification products were visualized via electrophoresis using 2% agarose gel.

Primers (5' > 3') for single-cell RT-PCR were as follows. GAPDH (sense/anti-sense): multiplex, ACTCCACTCACGGCAAATTC/CACATTGGGGGTAGGAACAC; nested, AGCTTGTTCATCAACGGGAAG/GTCATGAGCCCTTCACAAT; final product 331 base pairs (bp). GAD1 (sense/anti-sense): multiplex, CACAGGTCAACCCTCGATTTT/TCTATGCCGCTGAGTTTGTG; nested, TAGCTGTGAATGGCTGACA/CTTGTAACGAGCAGCCATGA; final product 200 bp. VGLUT2 (sense/anti-sense): multiplex, GCCGCTACATCATAGCCATC/GCTCTCTCCAATGCTCTCCTC; nested, ACATGGTCAACAACAGCACTATC/ATAAGACACCAAGGAGCCAGAAC; final product 506 bp. HDC (sense/anti-sense): multiplex, GGAGCCCTGTGAATACCGTG/TCCACTGAAGAGTGAGCCTGA; nested, CGTGAATACTACCGAGCTAGAGG/ACTCGTTCAATGTCCCCAAAG; final product 182 bp. These procedures are related to the results in Extended Data Fig. 2.

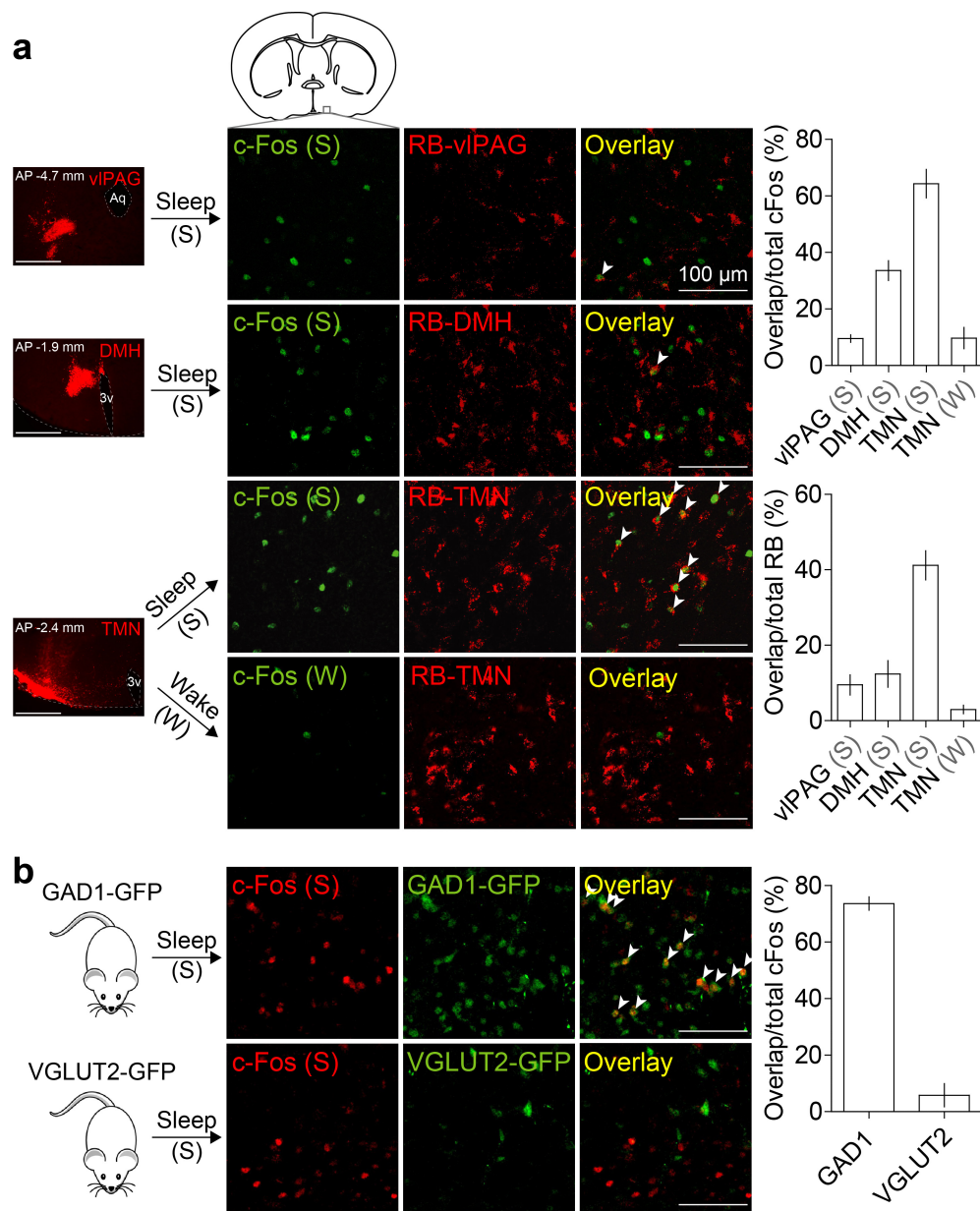
Statistics. Statistical analysis was performed using MATLAB, GraphPad Prism, or Python. The selection of statistical tests was based on reported previous studies. All statistical tests were two-sided. The 95% confidence intervals for brain state probabilities were calculated using a bootstrap procedure: for an experimental group of *n* mice, with mouse *i* comprising *m_i* trials, we repeatedly resampled the data by randomly drawing for each mouse *m_i* trials (random sampling with replacement). For each of the 10,000 iterations, we recalculated the mean probabilities for each brain state across the *n* mice. The lower and upper confidence intervals were then extracted from the distribution of the resampled mean values. To test whether a given brain state was significantly modulated by laser stimulation, we calculated for each bootstrap iteration the difference between the mean probabilities during laser stimulation and the preceding period of identical duration. The investigators were not blinded to allocation during experiments and outcome assessment.

Sample size. To determine the sample size for optogenetic and pharmacogenetic experiments, we first performed pilot experiments with two or three mice. Given the strength of the effect and the variance across this group, we then predicted the number of animals required to reach sufficient statistical power. To determine the sample size (number of units) for optrode recordings, we first recorded from two animals. Given the success rate of finding identified units and the homogeneity of units in the initial data set, we set a target sample size. For rabies-mediated

retrograde tracing, histology, and slice recording experiments, the selection of the sample size was based on numbers reported in previous studies. For gene profiling experiments, sample size was not calculated *a priori*, and the selection of the sample size was based on previous studies. Otherwise, no statistical methods were used to predetermine sample size.

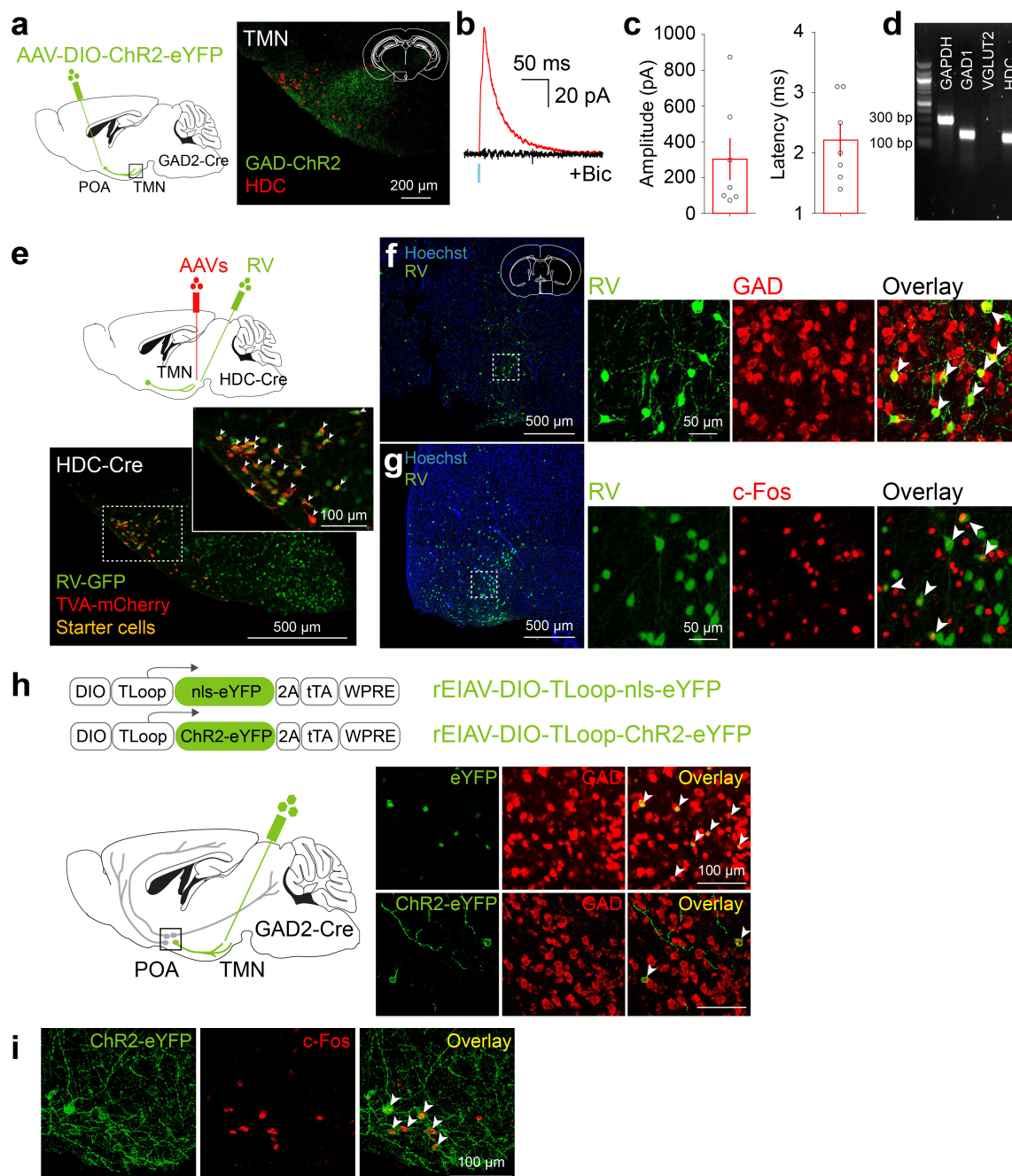
Data availability. The single-cell RNA-seq data have been deposited in the Gene Expression Omnibus under accession number GSE79108. All other data are available from the corresponding author upon reasonable request.

32. Vong, L. *et al.* Leptin action on GABAergic neurons prevents obesity and reduces inhibitory tone to POMC neurons. *Neuron* **71**, 142–154 (2011).
33. Madisen, L. *et al.* A robust and high-throughput Cre reporting and characterization system for the whole mouse brain. *Nat. Neurosci.* **13**, 133–140 (2010).
34. Krashes, M. J. *et al.* An excitatory paraventricular nucleus to AgRP neuron circuit that drives hunger. *Nature* **507**, 238–242 (2014).
35. Terao, A., Greco, M. A., Davis, R. W., Heller, H. C. & Kilduff, T. S. Region-specific changes in immediate early gene expression in response to sleep deprivation and recovery sleep in the mouse brain. *Neuroscience* **120**, 1115–1124 (2003).
36. Borbély, A. A., Tobler, I. & Hanagasioglu, M. Effect of sleep deprivation on sleep and EEG power spectra in the rat. *Behav. Brain Res.* **14**, 171–182 (1984).
37. Anikeeva, P. *et al.* Optetrode: a multichannel readout for optogenetic control in freely moving mice. *Nat. Neurosci.* **15**, 163–170 (2011).
38. Schmitzer-Torbert, N., Jackson, J., Henze, D., Harris, K. & Redish, A. D. Quantitative measures of cluster quality for use in extracellular recordings. *Neuroscience* **131**, 1–11 (2005).
39. Knight, Z. A. *et al.* Molecular profiling of activated neurons by phosphorylated ribosome capture. *Cell* **151**, 1126–1137 (2012).
40. Mi, H., Muruganujan, A., Casagrande, J. T. & Thomas, P. D. Large-scale gene function analysis with the PANTHER classification system. *Nat. Protocols* **8**, 1551–1566 (2013).
41. Sugino, K. *et al.* Molecular taxonomy of major neuronal classes in the adult mouse forebrain. *Nat. Neurosci.* **9**, 99–107 (2006).
42. Hempel, C. M., Sugino, K. & Nelson, S. B. A manual method for the purification of fluorescently labeled neurons from the mammalian brain. *Nat. Protocols* **2**, 2924–2929 (2007).
43. Tasic, B. *et al.* Adult mouse cortical cell taxonomy revealed by single cell transcriptomics. *Nat. Neurosci.* **19**, 335–346 (2016).
44. Zhang, S. *et al.* Long-range and local circuits for top-down modulation of visual cortex processing. *Science* **345**, 660–665 (2014).
45. Lambolez, B., Audinat, E., Bochet, P., Crépel, F. & Rossier, J. AMPA receptor subunits expressed by single Purkinje cells. *Neuron* **9**, 247–258 (1992).



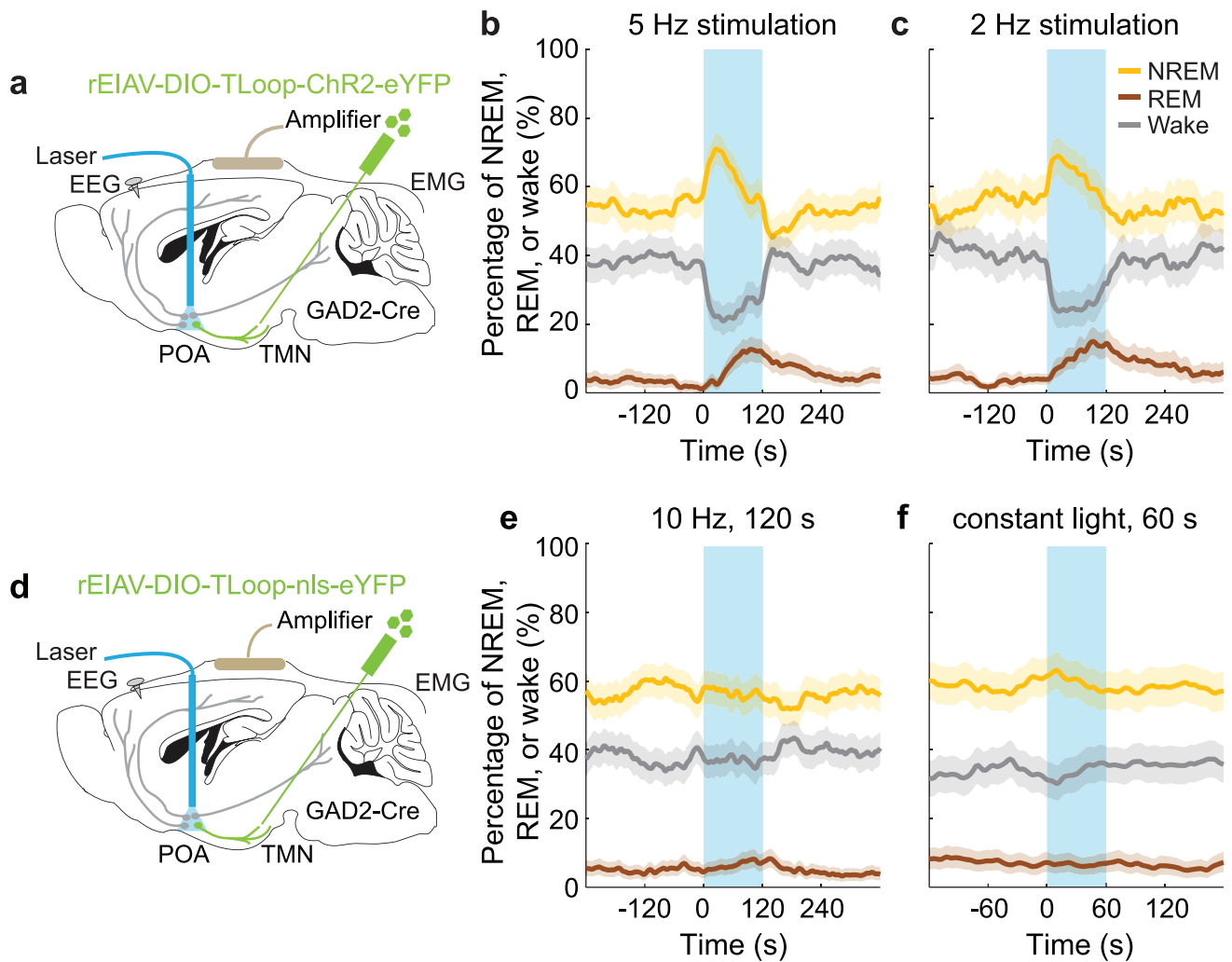
Extended Data Figure 1 | Overlap of c-Fos staining of sleep-active POA neurons with retrograde labelling from several brain regions and with GAD1-GFP or VGLUT2-GFP. a, Overlap between c-Fos expression induced by sleep rebound (Sleep, $n = 5$ mice) or sleep deprivation (Wake, $n = 3$) and retrobead (RB) labelling from the TMN, dorsomedial hypothalamus (DMH, $n = 3$), or ventrolateral periaqueductal grey (vIPAG, $n = 3$). Mouse brain figure adapted with permission from ref. 31. Left column, representative images showing retrobead injection sites (scale bars, 500 μm). Percentage of c-Fos⁺ neurons containing retrobead and

percentage of retrobead-containing cells that were c-Fos⁺ were both significantly different among target regions ($P < 0.0001$ and $P = 0.0004$, one-way analysis of variance followed by Dunnett's post-hoc test). Many retrobead-labelled neurons from TMN expressed c-Fos following sleep but not following wake. **b,** Overlap between c-Fos expression induced by sleep rebound and GAD1-GFP (top, five mice) or VGLUT2-GFP (bottom, three mice). Many c-Fos⁺ cells were GAD1⁺ (arrowheads). Error bar, \pm s.e.m.



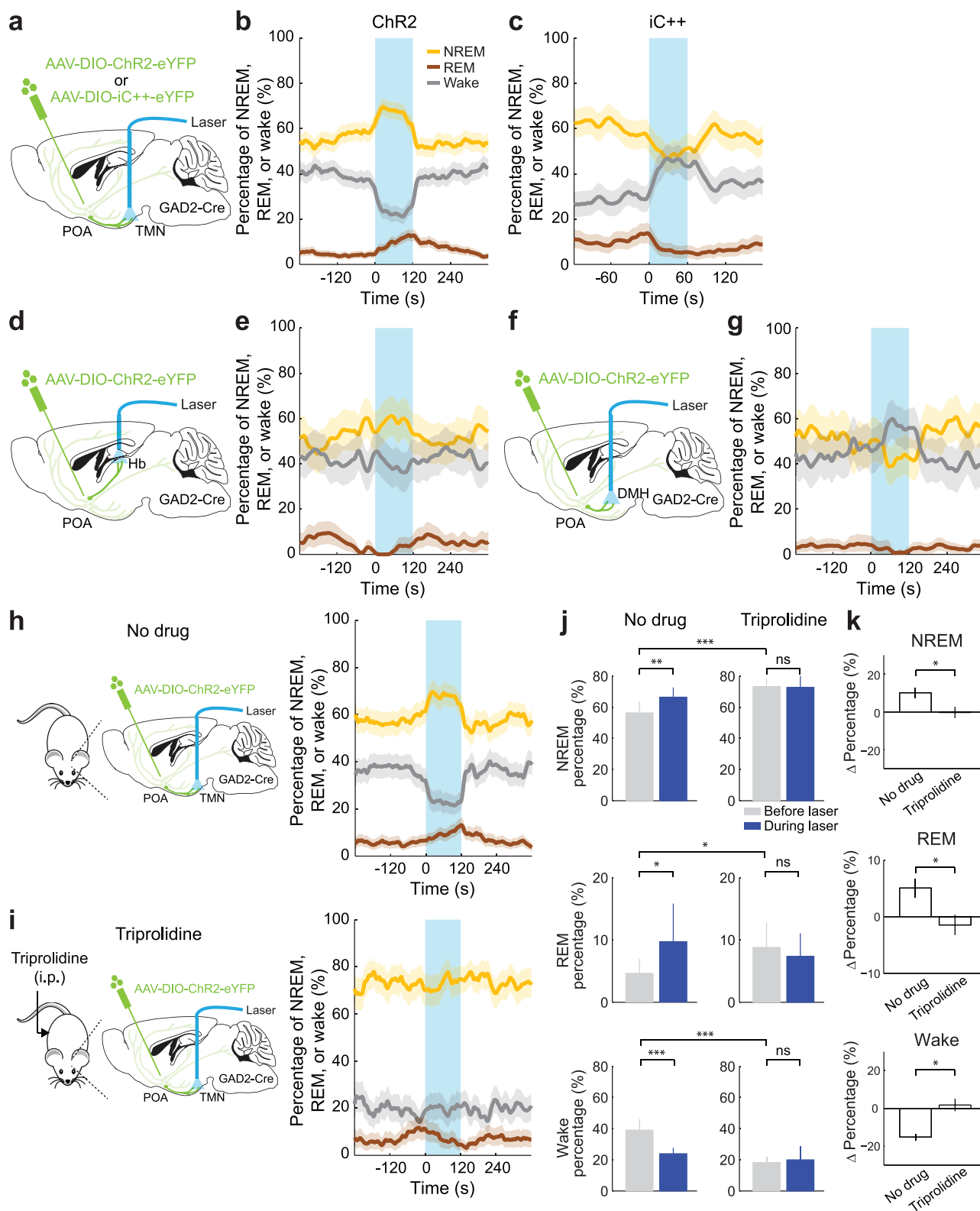
Extended Data Figure 2 | Innervation of histamine neurons in the TMN by GABAergic neurons in the POA and overlap of lentivirus labelling of $GABA^{POA \rightarrow TMN}$ neurons with GAD expression and with c-Fos labelling after sleep rebound. **a**, In GAD2-Cre mice injected with AAV-DIO-ChR2-eYFP in the POA (left), ChR2-eYFP-expressing axons (green) are observed in the TMN area (red, histidine decarboxylase (HDC)). Mouse brain figure adapted with permission from ref. 31. **b**, Inhibitory postsynaptic current (red) recorded in an example TMN histamine neuron, evoked by optogenetic activation of POA GABAergic axons. Light-evoked responses (red) were blocked by bicuculline (black). Blue tick, laser stimulus. **c**, Amplitudes and latencies of inhibitory postsynaptic currents recorded from TMN histamine neurons ($n = 7$, from two mice). Each symbol represents data from one cell. Error bar, \pm s.e.m. **d**, Single-cell RT-PCR identification of HDC-expressing histamine neurons. **e**, Schematic of RV-mediated trans-synaptic retrograde tracing from TMN histamine neurons. Fluorescence image of the TMN shows starter cells (yellow, expressing both GFP and mCherry). Inset, enlarged view of the region in white box. **f**, Left, fluorescence image showing input neurons in the POA. Right, enlarged view of the

region in white box, showing RV-GFP labelling (green) and GAD1/2 expression (red, FISH for mRNA encoding GAD1/2). Arrowheads, RV labelled cells that are GAD1/2⁺. $79.0 \pm 1.4\%$ of RV-GFP labelled neurons contained mRNA encoding GAD1/2 ($n = 2$ mice). **g**, Overlap between c-Fos expression induced by sleep rebound and RV-GFP labelling. Left, fluorescence image showing input neurons in the POA. Right, enlarged view of the region in white box, showing RV-GFP labelling and c-Fos expression; $46.9 \pm 1.9\%$ of RV-GFP labelled neurons expressed c-Fos ($n = 6$ mice). **h**, Expression of eYFP or ChR2-eYFP in the POA induced by injecting rEIAV-DIO-TLoop-nls-eYFP or rEIAV-DIO-TLoop-ChR2-eYFP into the TMN of GAD2-Cre mice and their overlap with GAD1/2 expression (FISH for mRNA encoding GAD1/2). Arrowheads indicate cells co-labelled with GAD-FISH probe and eYFP or ChR2-eYFP; $96.2 \pm 1.4\%$ of eYFP-labelled neurons and $95.4 \pm 3.7\%$ of ChR2-eYFP-labelled neurons contained mRNA encoding GAD1/2 ($n = 4, 5$). **i**, Expression of ChR2-eYFP in the POA induced by injecting rEIAV-DIO-TLoop-ChR2-eYFP into the TMN of a GAD2-Cre mouse and its overlap with c-Fos expression following sleep rebound (arrowheads).



Extended Data Figure 3 | Effect of optogenetic activation of $GABA^{POA \rightarrow TMN}$ neurons at low frequencies and effect of laser stimulation in $GABA^{POA \rightarrow TMN}$ -eYFP control mice. **a**, Similar to Fig. 1, rEIAV-DIO-TLoop-ChR2-eYFP was injected into the TMN of GAD2-Cre mice and an optic fibre was implanted into the POA for optogenetic stimulation. Mouse brain figure adapted with permission from ref. 31. **b**, Percentage of time the mice spent in wake, NREM, or REM state before, during, and after laser stimulation (blue shading, 5 Hz, 120 s), averaged from five mice ($P < 0.0001$ for wake, REM, and NREM, bootstrap). **c**, Similar to **b**, but with 2 Hz stimulation ($P < 0.0001$ for wake and REM,

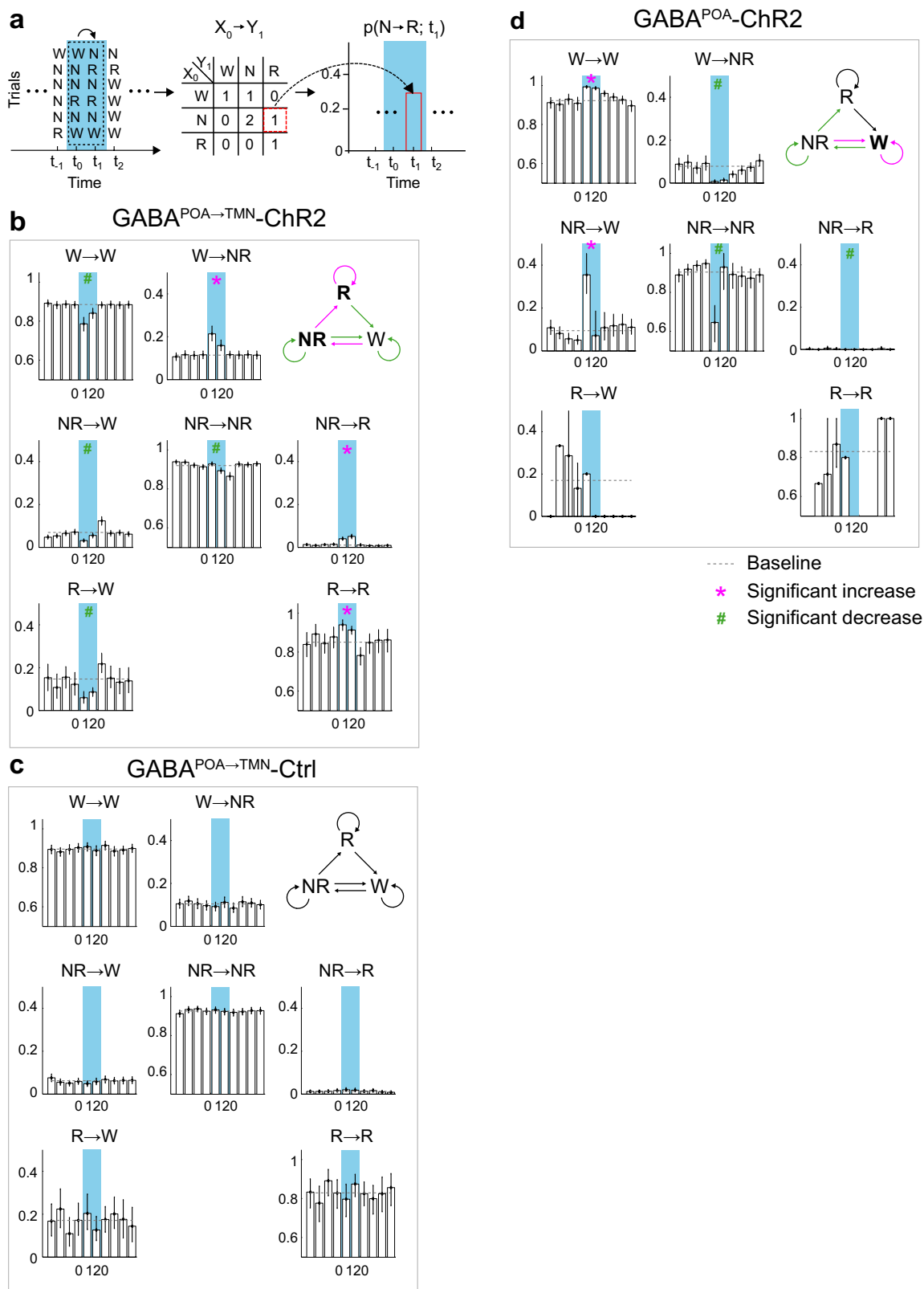
$P = 0.002$ for NREM, bootstrap, $n = 5$ mice). **d**, Similar to **a**, after rEIAV-DIO-TLoop-nls-eYFP injection. **e**, Effect of 10 Hz stimulation in eYFP control mice. Shown is the percentage of time in wake, NREM, or REM state before, during, and after laser stimulation (blue shading, 10 Hz, 120 s), averaged from eight mice ($P = 0.18, 0.84$, and 0.35 for REM, NREM, and wake respectively, bootstrap). **f**, Effect of constant light stimulation (blue shading, constant light, 60 s), averaged from five mice ($P = 0.57, 0.27$, and 0.73 for REM, NREM, and wake, bootstrap). Shading for each trace, 95% confidence interval.



Extended Data Figure 4 | See next page for caption.

Extended Data Figure 4 | Optogenetic manipulation of axon projections of GABA^{POA} neurons to TMN, dorsomedial hypothalamus, and habenula, and effect of anti-histamine on optogenetic activation of the TMN axon projections. **a**, AAV-DIO-ChR2-eYFP or AAV-DIO-iC⁺⁺-eYFP was injected into the POA of GAD2-Cre mice and an optic fibre was implanted into the TMN for optogenetic activation/inhibition. Mouse brain figure adapted with permission from ref. 31. **b**, Percentage of time in wake, NREM, or REM state before, during, and after laser stimulation (blue shading, 10 Hz, 120 s) in mice expressing ChR2, averaged from nine mice ($P < 0.0001$ for wake, REM and NREM, bootstrap). Shading for each trace, 95% confidence interval. **c**, Similar to **b**, but in mice expressing iC⁺⁺ (blue shading: constant light, 60 s), averaged from four mice ($P < 0.0001$ for wake and NREM, $P = 0.004$ for REM, bootstrap). **d**, Schematic for optogenetic activation of POA GABAergic projection to the habenula (Hb). **e**, Similar to **b**, for activating POA→habenula projection ($P = 0.28, 0.35$ and 0.72 for REM, wake and NREM, bootstrap, $n = 3$ mice). **f**, Schematic for optogenetic activation of POA GABAergic projection to the dorsomedial

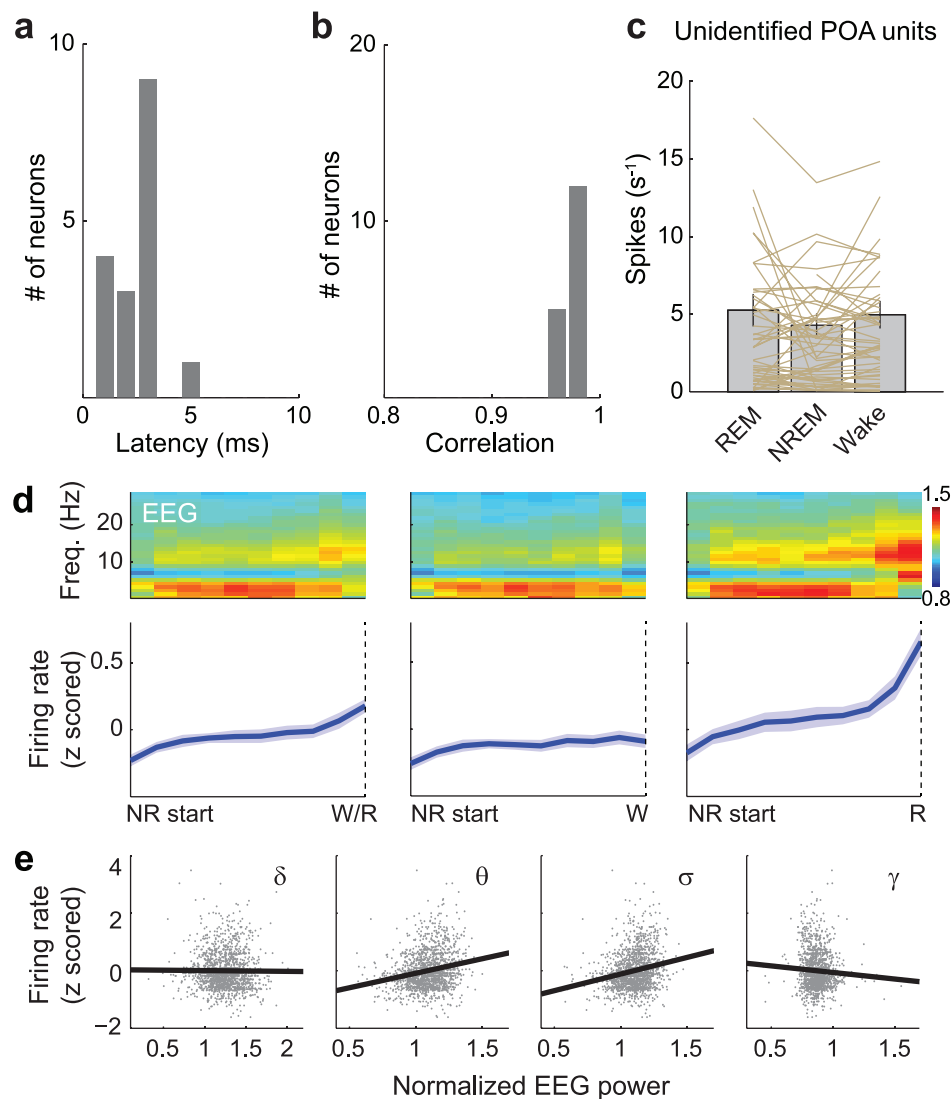
hypothalamus. **g**, Similar to **b**, for POA→dorsomedial hypothalamus activation ($P = 0.02, 0.12$, and 0.09 for wake, REM, and NREM, $n = 3$ mice). **h**, Left, schematic for optogenetic activation of POA GABAergic projection to the TMN without drug treatment. Right, percentage of time in wake, NREM, or REM state before, during, and after laser stimulation (blue shading, 10 Hz, 120 s) in mice with no drug (effect of laser: $P < 0.001$ for wake, REM, and NREM, bootstrap; $n = 14$ mice). **i**, Similar to **h**, but after intraperitoneal injection of triprolidine (20 mg per kg (body weight)); effect of laser: $P = 0.21, 0.84, 0.57$ for wake, REM, and NREM, $n = 5$ mice). **j**, Percentage of time in NREM, REM, or wake state before and during laser stimulation in no drug and triprolidine groups (120 s periods before and during laser stimulation, $*P < 0.05$, $**P < 0.01$, $***P < 0.001$; NS, $P > 0.05$, signed rank test between before and during laser, rank sum test between no drug and triprolidine for the period before laser stimulation). **k**, Laser-induced change in the percentage of each state (difference between the 120 s periods before and during laser stimulation, $*P < 0.05$, rank sum test). Error bar, \pm s.e.m.



Extended Data Figure 5 | See next page for caption.

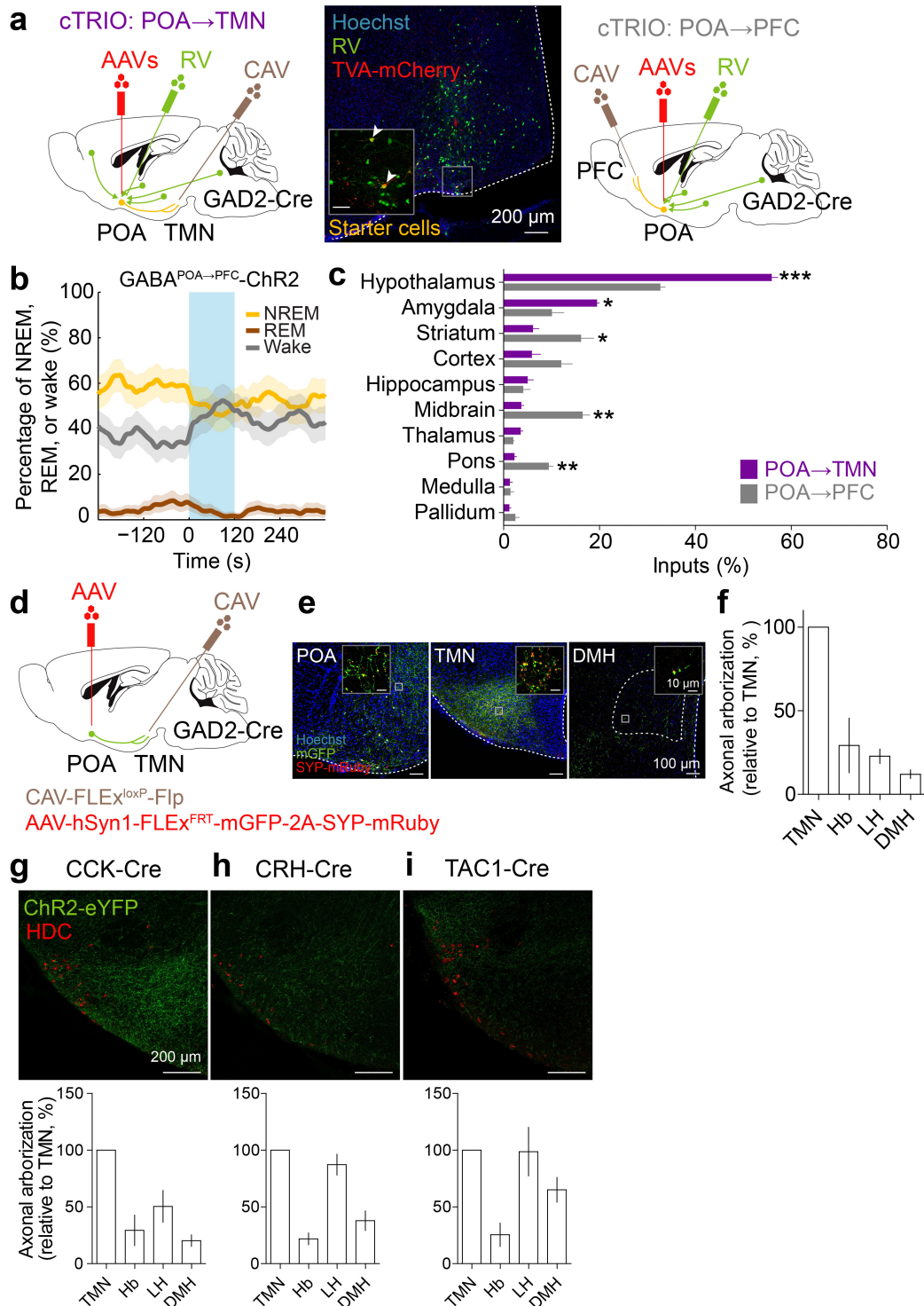
Extended Data Figure 5 | Effect of laser stimulation on transition probability between each pair of brain states in GABA^{POA→TMN}-ChR2, GABA^{POA→TMN}-Ctrl, and GABA^{POA}-ChR2 mice. **a**, Schematic showing transition probability calculation. To calculate the transition probability at a given time bin (i), we first identified all the trials (n) in which the animal was in state X (X could be wake, NREM, or REM) in the preceding time bin ($i - 1$). Among these n trials, we identified the subset of trials (m) in which the animal transitioned into state Y in the current time bin (i). The $X \rightarrow Y$ transition probability for time bin i was computed as m/n . **b**, Transition probability within each 10 s period in GABA^{POA→TMN}-ChR2 mice ($n = 9$). Shown in each bar is the transition probability averaged across six consecutive 10 s bins within each 60 s. Error bar, 95% confidence

interval (bootstrap). The baseline transition probability (grey dashed line) was averaged across all time bins after excluding the laser stimulation period. Direct wake \rightarrow REM and REM \rightarrow NREM transitions were not observed and the corresponding plots were omitted. Magenta asterisk (*) / green hash symbol (#) indicates significant increase/decrease in transition probability during laser stimulation compared with the baseline ($P < 0.05$, bootstrap). Top right diagram indicates transition probabilities that are significantly increased (magenta), decreased (green), or unaffected (black) by laser stimulation. **c**, Transition probability in control mice ($n = 8$). The probability during laser stimulation was not significantly different from baseline for any transition. **d**, Transition probability in GABA^{POA}-ChR2 mice ($n = 5$).



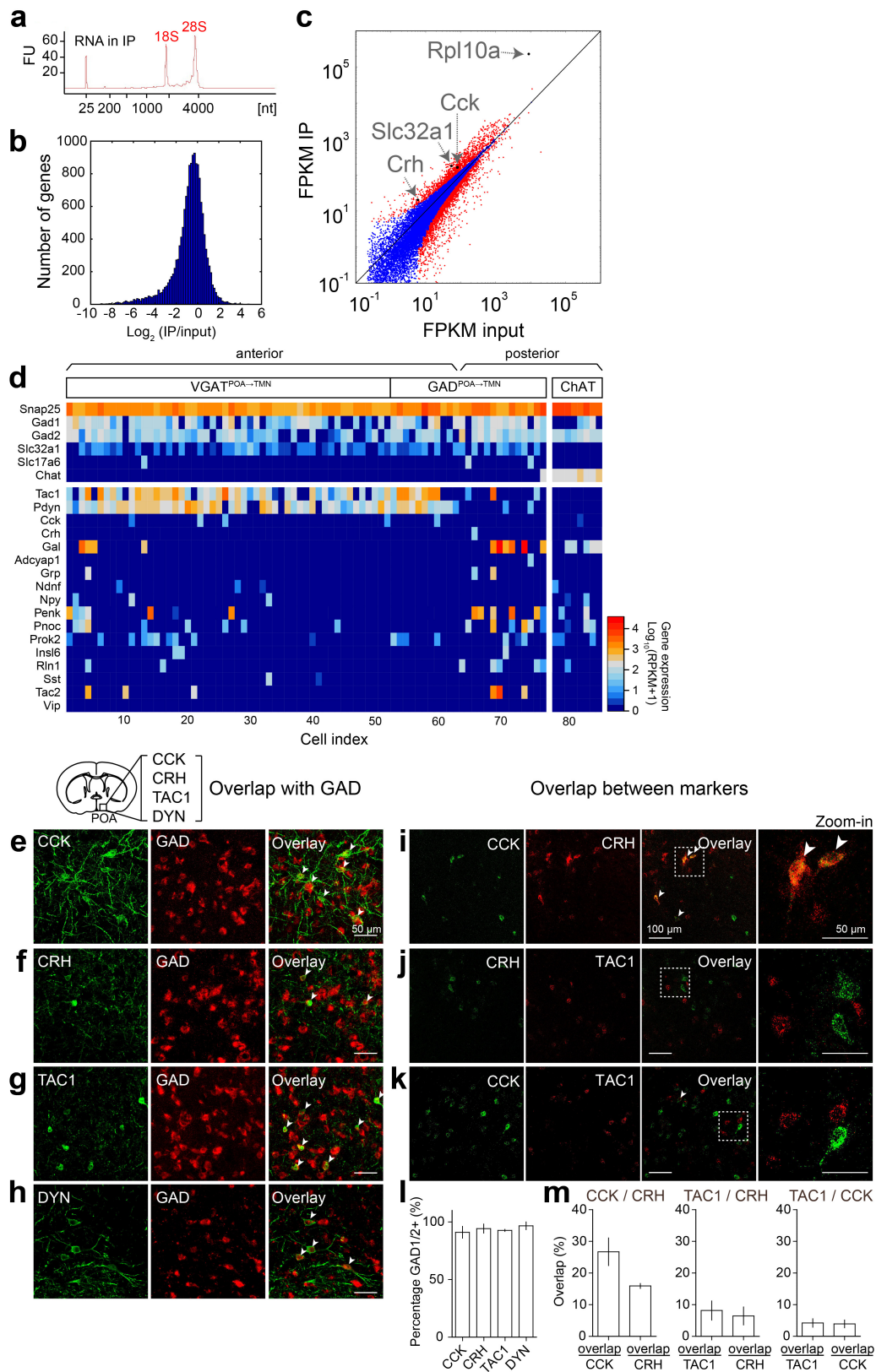
Extended Data Figure 6 | Optogenetic identification of GABA^{POA→TMN} neurons, firing rates of unidentified POA neurons, and firing rate dynamics of identified GABA^{POA→TMN} neurons during NREM sleep. **a**, Distribution of delays in laser-evoked spiking for all identified neurons. Delay was defined as timing of the first spike after each laser pulse. **b**, Distribution of correlation coefficient between laser-evoked and spontaneous spike waveforms for all identified neurons. **c**, Firing rates of unidentified units in the three brain states. Each line represents data from one neuron. Grey bar represents average over units ($n = 51$, from 11 mice). Error bar, \pm s.e.m. **d**, Firing rate change of identified GABA^{POA→TMN} neurons during each NREM episode. Top: mean EEG power spectrogram from start to end of each NREM episode. Bottom: mean firing rate of the recorded neurons. Left: average across all NREM episodes. Each NREM period was divided into ten time bins (temporally normalized). The firing rate of each neuron was z-scored and averaged across all recorded NREM episodes. Solid line, mean of 17 neurons; shading, \pm s.e.m. To test significance of the firing rate increase during NREM episodes, for each unit we measured the slope of its mean firing

rate versus time after NREM onset, as quantified by a linear fit. Across the 17 units recorded, the increase (slope > 0) was significant ($P = 1.0 \times 10^{-5}$, t -test). Middle and right: similar to left, for the subset of NREM episodes preceding wakefulness ($P = 0.0089$) and that preceding REM sleep ($P < 10^{-5}$). The increase in firing rate was stronger for NREM episodes preceding REM sleep than those preceding wakefulness ($P = 0.0003$, paired t -test). **e**, Correlation between firing rate and EEG power in different frequency bands (delta, 0.5–4 Hz; theta, 4–12 Hz; sigma, 9–25 Hz; gamma, 40–120 Hz) during NREM sleep. The firing rate of each neuron was z-scored, and the power within each frequency band was normalized by its mean across each recording session. Firing rates and EEG power in each frequency band were discretized in 2.5 s bins. For each bin assigned to NREM sleep, we plotted the power in each frequency bands versus the corresponding firing rate. Linear regression was used to determine whether the power in each frequency band and the firing rate were positively or negatively correlated. The correlation was positive for theta ($P < 10^{-5}$) and sigma ($P < 10^{-5}$), negative for gamma ($P < 10^{-5}$), and not significant for delta ($P = 0.58$).



Extended Data Figure 7 | Mapping of monosynaptic inputs and axon projections of GABA^{POA→TMN} neurons and axon projections of POA CCK, CRH, TAC1 neurons. **a**, Schematic of cTRIO to map monosynaptic inputs to GABA^{POA→TMN} (left) or GABA^{POA→PFC} (right) neurons. Mouse brain figure adapted with permission from ref. 31. Middle, coronal section of a mouse brain at the POA stained with Hoechst (blue). A region within the square is magnified in the inset. Arrowheads indicate starter cells (yellow) at the injection site (scale bar in inset, 50 μm). **b**, Optogenetic activation of GABA^{POA→PFC} neurons. Shown is the percentage of time in wake, NREM, or REM state before, during, and after laser stimulation (blue shading, 10 Hz, 120 s), averaged from six mice ($P < 0.001$ for wake and NREM, $P = 0.003$ for REM, bootstrap). Shading for each trace, 95% confidence interval. **c**, Average fractional inputs in cTRIO^{POA→TMN} (purple) or cTRIO^{POA→PFC} (grey) tracing ($P = 0.0002$ for hypothalamus,

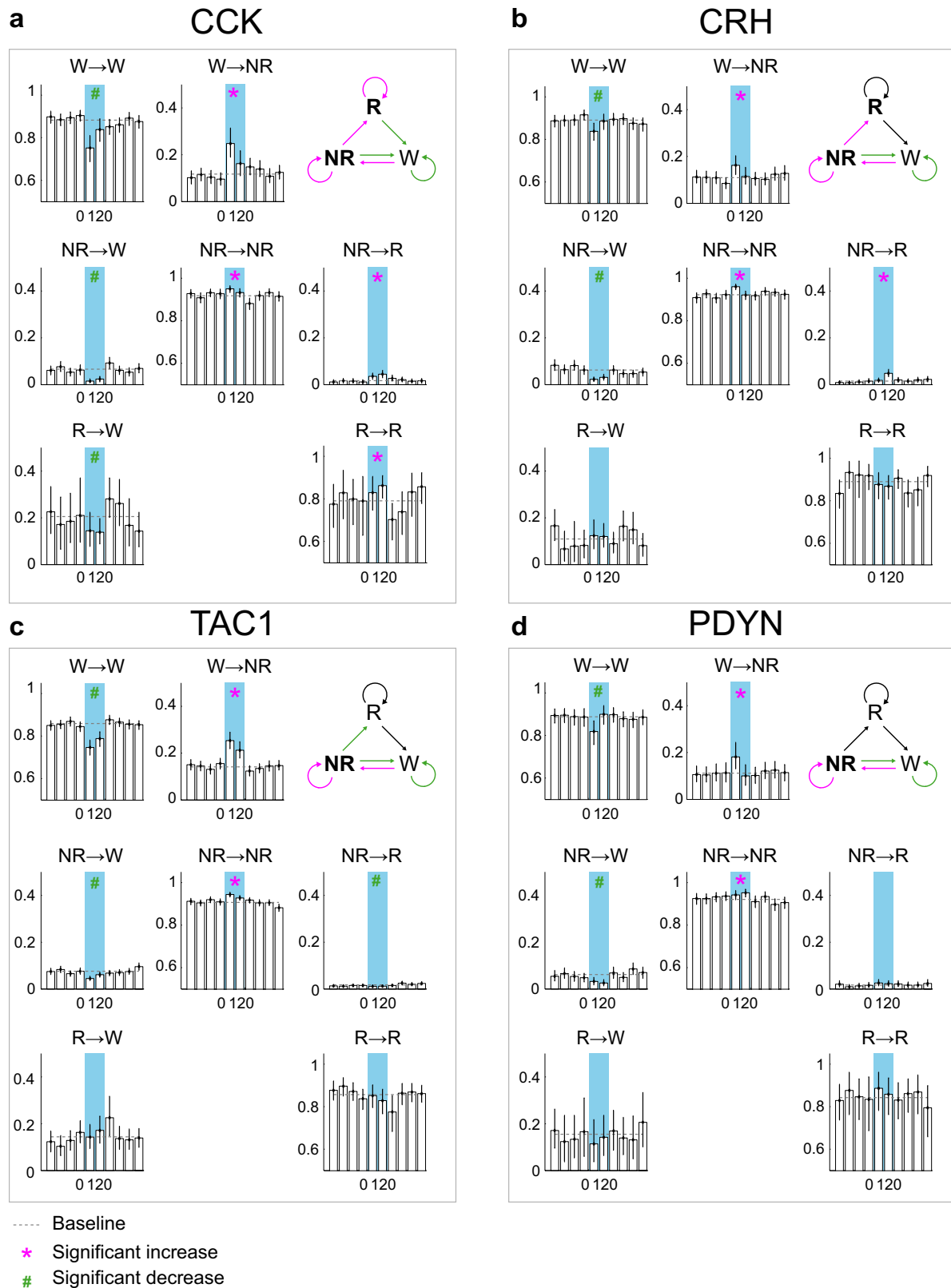
$P = 0.02$ for amygdala, $P = 0.03$ for striatum, $P = 0.001$ for midbrain, $P = 0.003$ for pons, t -test). $N = 3$ mice in each group. Error bar, \pm s.e.m. **d**, Schematic of the axon projection mapping experiment. **e**, Coronal sections containing POA, TMN, and dorsomedial hypothalamus regions stained with Hoechst (blue). A region within the square is magnified in the inset. Red, synaptophysin-mRuby; green, mGFP. **f**, Projection levels (quantified by mGFP-labelled axonal arbors) in different brain areas normalized by that in the TMN. Shown are only areas with projections $>10\%$ of the TMN projection. Hb, habenula; LH, lateral hypothalamus. $N = 3$ mice. **g–i**, Axon projections of POA CCK, CRH, TAC1 neurons. Top: coronal section containing the TMN region. Red, immunostaining for HDC showing histaminergic neurons. Bottom: projection levels (quantified by eYFP-labelled axonal arbors) in different brain areas normalized by that in the TMN. $N = 3, 3, 4$ mice respectively.



Extended Data Figure 8 | See next page for caption.

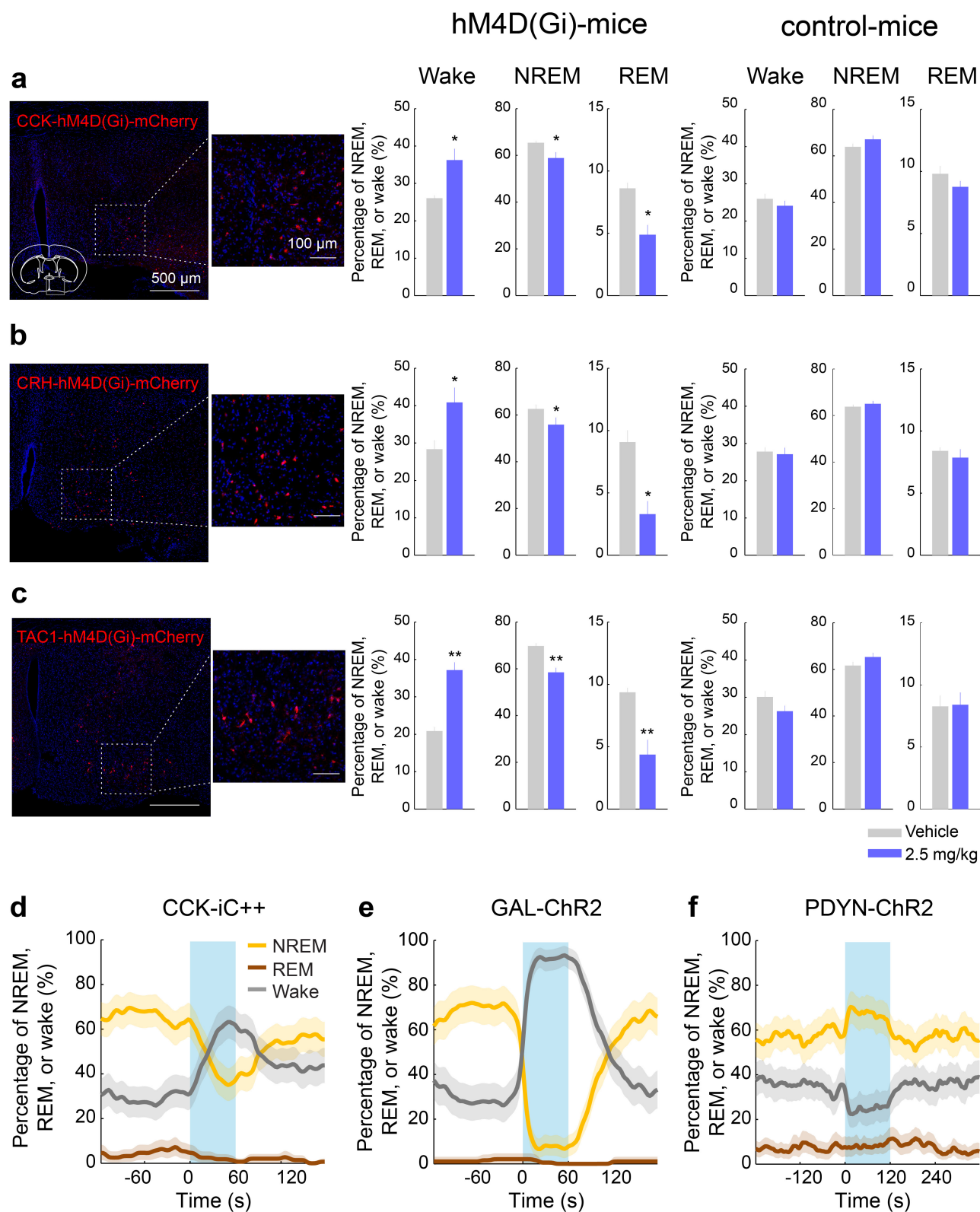
Extended Data Figure 8 | Identification of genetic markers for GABA^{POA→TMN} neurons using TRAP and single-cell RNA-seq, and overlap between each identified marker and GAD and between the markers in the POA. **a**, TRAP; shown is bioanalyzer trace of immunoprecipitated RNA. FU, fluorescence units. **b**, Histogram display of differentially expressed genes (immunoprecipitation per input). **c**, Fragments per kilobase of transcript per million mapped reads (FPKM) immunoprecipitation versus FPKM input (log scale). Several marker genes enriched in GABA^{POA→TMN} neurons (Cck, Crh, Slc32a1, Rpl10a) are highlighted. Red dots, genes that are significantly different in immunoprecipitation versus input ($P < 0.05$, Fisher's exact test); blue dots, non-significant genes. **d**, Single-cell RNA-seq; shown is heat map of expression levels of several cell-type markers (for example, Gad1, Gad2, Slc32a1, Slc17a6, and Chat) and all neuropeptide-encoding genes (on the basis of the list of ref. 43 plus GAL) in cholinergic neurons in the nucleus

basalis and eYFP-labelled GABA^{POA→TMN} neurons in the POA. Tac1 and Pdyn are highly expressed in GABA^{POA→TMN} neurons. RPKM, reads per kilobase of transcript per million mapped reads. **e–h**, Overlap between each identified marker and GAD. A representative image showing overlap between CCK-ChR2-eYFP (**e**), CRH-eYFP (**f**), TAC1-eYFP (**g**), DYN-ChR2-eYFP (**h**), and FISH for mRNA encoding GAD1/2. Arrowheads indicate cells co-labelled with GAD1/2 probe and eYFP. Mouse brain figure adapted with permission from ref. 31. **i–k**, Overlap between the markers. A representative image showing overlap between CCK and CRH (**i**), CRH and TAC1 (**j**), or CCK and TAC1 (**k**) using double FISH for both peptides. Arrowheads indicate co-labelled cells. **l**, Percentage of cells expressing each peptide marker that are GAD1/2 positive ($n = 2$ or 3 mice per marker). **m**, Quantification of overlap between CCK and CRH, TAC1 and CRH, or TAC1 and CCK ($n = 3$ mice per pair). Error bar, \pm s.e.m.



Extended Data Figure 9 | Effect of laser activation of CCK, CRH, TAC1, and PDYN neurons on transition probability between each pair of brain states. a, Transition probability within each 10 s period in

CCK neuron activation experiment. Error bar, 95% confidence interval (bootstrap). $N = 4$ mice. **b–d,** Similar to **a**, for CRH, TAC1, and PDYN neuron activation. $N = 5, 7, 5$ mice, respectively.



Extended Data Figure 10 | See next page for caption.

Extended Data Figure 10 | Pharmacogenetic inactivation of CCK, CRH, and TAC1 neurons, optogenetic inactivation of CCK neurons, optogenetic activation of GAL neurons, and optogenetic activation of PDYN neurons in the POA. **a**, Pharmacogenetic inactivation of CCK neurons. Left, a representative image showing hM4D(Gi)-mCherry expression in the POA of a CCK-Cre mouse and an enlarged view of the region in white box. Mouse brain figure adapted with permission from ref. 31. Middle, effect of CNO injection in CCK-Cre mice expressing hM4D(Gi). Each bar shows the percentage of time in each brain state during the first 4 h of the recording session, after injection of vehicle (grey) or CNO (blue). Error bar, \pm s.e.m. ($n = 6$ mice, $P = 0.022, 0.025, 0.044$ for REM, wake, and NREM, paired t -test). Right, effect of CNO injection in control CCK-Cre mice not expressing hM4D(Gi) ($n = 4$ mice, $P = 0.27, 0.46, \text{ and } 0.29$ for REM, wake, and NREM, paired t -test). The effect of CNO was significantly different between hM4D(Gi)-expressing and control mice ($P = 0.006, 0.036, \text{ and } 0.014$ for REM, wake, and NREM,

t -test). **b**, Similar to **a**, for CRH neuron inactivation ($n = 6$ mice, $P = 0.015, 0.018, 0.024$). For control, $n = 5$ mice; $P = 0.58, 0.41, \text{ and } 0.12$. Difference between hM4D(Gi) and control, $P = 0.003, 0.03, \text{ and } 0.014$. **c**, For TAC1 neuron inactivation ($n = 6$ mice, $P = 0.0057, 0.0026, 0.0095$). For control, $n = 4$ mice; $P = 0.92, 0.13, \text{ and } 0.06$. Difference between hM4D(Gi) and control, $P = 0.001, 0.005, \text{ and } 0.037$. **d**, Optogenetic inhibition of POA CCK neurons suppresses sleep and enhances wakefulness. Shown is the percentage of time in wake, NREM, or REM state before, during, and after laser stimulation (blue shading, constant light, 60 s), averaged from four mice ($P < 0.0001$ for wake and NREM, $P = 0.008$ for REM, bootstrap). **e**, Similar to **d**, with laser stimulation of POA GAL neurons (blue shading, 10 Hz, 60 s), averaged from four mice ($P < 0.0001$ for increase in wakefulness, bootstrap). **f**, Similar to **d**, with optogenetic stimulation of POA PDYN neurons (blue shading, 10 Hz, 120 s), averaged from five mice ($P = 0.42, 0.002, \text{ and } 0.0003$ for REM, NREM, and wake, bootstrap). Shading for each trace, 95% confidence interval.